Automated Detection of Covid-19 from HRCT Images using Deep Learning

Author

Ujala Gulzaib

Regn Number

00000318291

Supervisor

Dr. Amer Sohail Kashif

DEPARTMENT OF BIOMEDICAL ENGINEERING AND SCIENCES

SCHOOL OF MECHANICAL & MANUFACTURING ENGINEERING

NATIONAL UNIVERSITY OF SCIENCES AND TECHNOLOGY

ISLAMABAD, PAKISTAN

October 2022

Automated Detection of Covid-19 from HRCT Images using Deep Learning

Author

Ujala Gulzaib

Regn Number

00000318291

A thesis submitted in partial fulfillment of the requirements for the degree of

MS Biomedical Sciences

Thesis Supervisor:

Dr. Amer Sohail Kashif

Thesis Supervisor's Signature:

_____

DEPARTMENT OF BIOMEDICAL ENGINEERING AND SCIENCES

SCHOOL OF MECHANICAL & MANUFACTURING ENGINEERING

NATIONAL UNIVERSITY OF SCIENCES AND TECHNOLOGY

ISLAMABAD, PAKISTAN

October 2022

Copyright Statement

Dedication

Dedicated to my beloved Parents
‘Mr. & Mrs. Gulzaib’

Acknowledgments

First and foremost, I am thankful to Allah Subhana-Watala, the Most Gracious and Most Merciful for His blessings given to me and to have guided me throughout this work. I could have nothing without Your priceless help and guidance. Whosever helped me throughout the course of my thesis, whether my parents, siblings, and friends were Your will, so indeed none be worthy of praise but you.

I am profusely thankful to my beloved parents and my grandfather (late) who raised me when I was not capable of walking and continued to support me throughout in every step of my life.

I would like to express my profound gratitude and special thanks to my supervisor Dr. Amer Sohail Kashif, for his unwavering support and advice during my thesis, as well as for providing me with resources for my research. I am thankful to him for assisting me in learning and for giving me his precious time and attention.

I am especially thankful to Dr. Syed Omer Gillani for his tremendous support and cooperation. Each time I got stuck in something, he came up with solution. Without his support I wouldn't have been able to complete my thesis. I appreciate his patience and guidance throughout the whole thesis.

I am thankful to Dr. Asim Waris & Dr. Javaid Iqbal for their constant support and continuous guidance throughout the whole journey of this project. I really appreciate the compassion, kindness, and assistance of my all-thesis GEC members throughout my research work.

I am thankful to all siblings, my beloved brother and sisters for their treasured support and unwavering faith in me. They have always been a great source of inspiration for me. Special thanks to my Mujtaba, whose one smile was enough for me to keep me motivated all the tough time in hostel.

Finally, very wholeheartedly thanks to my beautiful friends Amna, Saman, Noor and more specially & specifically Zarqa for being there with me always and feel me like a family during this whole journey. I would like to express my gratitude to all individuals who have rendered valuable assistance to my study.


بسم الله الرحمن الرحيم

Abstract

Accurate and early diagnosis of coronavirus disease is essential for quick decision-making and patient management. Polymerase chain reactions (PCR) confirm Covid-19 but are limited due to prolonged execution time for analysis. Early disease detection is possible using High Resonance Computerized Tomography (HRCT) images as input in an automated disease prediction model. This is helpful for patients to take early precautionary measures even before consulting a radiologist. Different pre-trained deep neural networks have been used and higher accuracy has been achieved in this model. This study aims to detect disease more accurately and rapidly by differentiating between normal and infected images. The dataset available on Kaggle is divided into 70:15:15 ratios in which training, validation, and test dataset contain 18676, 4000, and 4000 images, respectively. Five different pre-trained deep neural networks ResNet50V2, MobileNetV2, EffecientNetB0, InceptionV3, and Xception Net are compared using an open-source data set to train and validate our proposed model. The proposed model achieves an overall accuracy of 99.9% on ResNet50V2 followed by 99.1% on MobileNetV2, 98.5% on Xception, 98.4% on Inception, and 94.1% on Efficient NetB0. Mobile NetV2 achieves the highest covid-19 sensitivity of 99.5% and ResNet50V2 gives 99.9% covid specificity among all other networks. In future, such prediction models can be used in clinical settings to develop computer-aided diagnosis (CAD) models for clinicians.

Keywords: Convolution Neural Network (CNN), Coronavirus, Covid-19, Deep Neural Network (DNN), HRCT Images

TABLE OF CONTENT

List of Figures

List of Tables

Abbreviations

AI	Artificial Intelligence
ARDS	Acute Respiratory Distress Syndrome
ALI	Acute Lung Injury
AUC	Area Under Curve
CNN	Convolutional Neural Network
COPD	Chronic Obstructive Pulmonary Disease
Covid-19	Coronavirus Disease 2019
CoV-2	Corona Virus 2
CT	Computed Tomography
DAD	Diffuse Alveolar Damage
DL	Deep Learning
DNN	Deep Neural Network
GGO	Ground Glass Opacity
HRCT	High Resonance Computerized Tomography
LL	Left Lung
ML	Machine Learning
RL	Right Lung
RT-PCR	Real Time Polymerase Chain Reactions
SARS	Severe Acute Respiratory Syndrome
SVM	Support Vector Machines
WHO	World Health Organization

CHAPTER 1

INTRODUCTION

INTRODUCTION

1.1 COVID-19

The novel coronavirus a global pandemic also known as COVID-19, caused by severe acute respiratory syndrome (SARS) coronavirus 2 (CoV-2), which belongs to SARS family (SARS-Cov-2). Tin December 2019, this disease initially occurred in Hubei province of Wuhan, China (Huang et al., 2020; Li et al., 2020). Covid-19 has high homology to SARS-CoV, approximately 80%, and caused acute respiratory distress syndrome (ARDS) in 2002-2003, with a high mortality rate (Ksiazek et al., 2003). China's seafood market in Wuhan is associated with zoonotic transmission of SARS-Coronavirus-2 outbreak. Studies recognized human-to-human transmission, as a major part of this subsequent outbreak (Tian et al., 2020). This virus caused a disease called Coronavirus disease in 2019 referred to as COVID-19, which by World Health Organization (WHO) was declared a global pandemic on 30th January 2020 (Sohrabi et al., 2020).

Studies reported impact of COVID-19 on a large population, in more than 200 countries and territories worldwide (Zhang et al., 2020). An estimated death rate due to this pandemic is between 1% to 5% (Ruan et al., 2020). Confirmed Covid cases have been reported around 526 million with 6.28 million total deaths as of 23rd May 2022 (Kurihara, 2022). About 80% of confirmed cases present mild symptoms such as headache, fever, breathing difficulties, cough, vomiting, generalized weakness, and diarrhea (Ruan et al., 2020). Severe cases presented with pneumonia, multiple organ failure, and ultimately death (Mahase, 2020). In Covid-19, majority of deaths occurred in immunocompromised patients above 60 years, or those with some preexisting conditions like heart diseases, and hypertension (Wu & McGoogan, 2020).

1.2 Lungs and Coronavirus Disease

Lungs are a pair spongy air-filled, primary organs of respiratory system that are located on either side of thorax. Right and left lung are separated from each other by mediastinum and are suspended by lung root. Depending upon their location in thorax, each lung has three surfaces. The costal surface, diaphragmatic surface, and mediastinal surface. A thin layer

of tissue known as pleura, provides cushion and protects the lungs. The windpipe known as trachea inhaled air through tubular branches (bronchi) into the lungs.

Bronchi divided into bronchioles which eventually ends in microscopic cluster of air sacs called as alveoli. The gaseous exchange (oxygen and carbon dioxide) takes place with the help of alveoli. SARS-CoV-2 filled the interstitial spaces with fluid that can lead to pneumonia, thus affects one or both lungs (Ruan et al., 2020). Lung is the main affected organ and its damage cause death in majority of covid-infected patients (Mahase, 2020).

1.2.1 Lungs Lobes

The two lungs right and left in body, are of different sizes. Right lung (RL) is greater than left one. Lung on each side of chest cavity is further divided into lobes and lobes are separated by fissures.

- Right Lung (RL) → 3 Lobes
- Left Lung (LL) → 2 Lobes

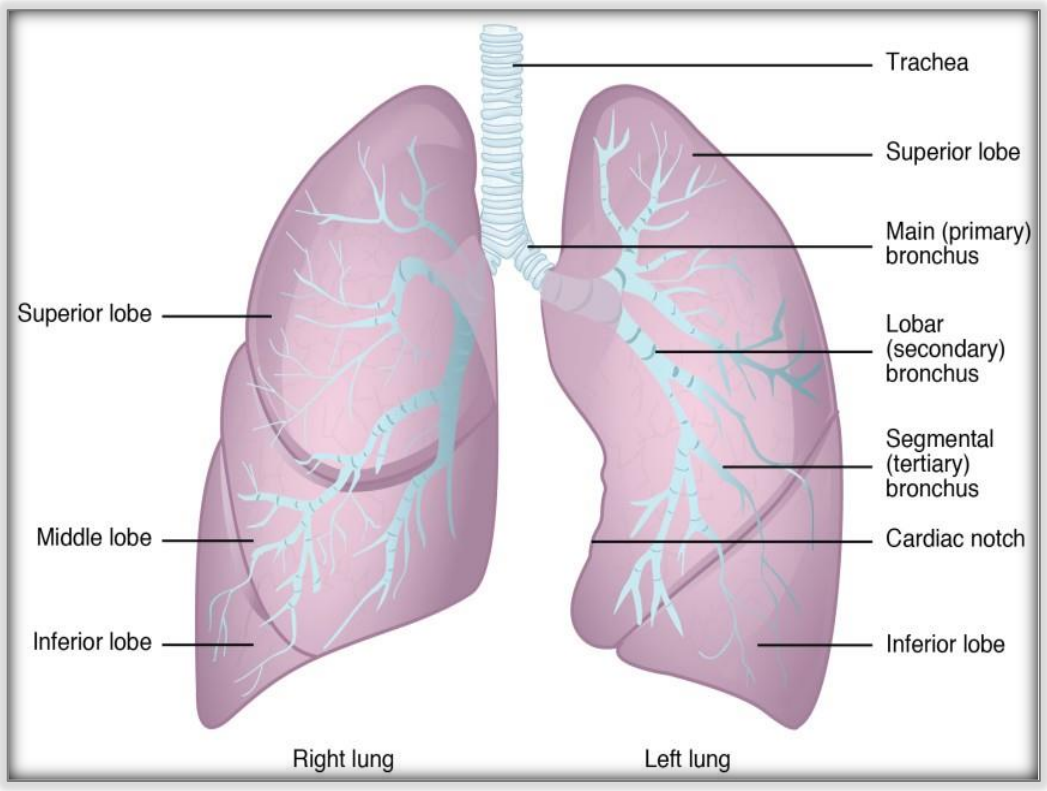

Figure 1: Lungs and their lobes. RL with three lobes and LL with two lobes

1.3 Pulmonary Pathology of Coronavirus

In most severe cases of coronavirus disease, one of the dominant features is pulmonary damage. Acute Lung injury (ALI) develop in patients frequently accompanied by coagulopathy which is also called pneumonia. In autopsy cohorts, elderly males with severe Covid-19 ranges from 31-96 years with a mean age of 73-81.5 years (Maiese et al., 2020; Omori et al., 2020). Most of individuals showed several comorbidities such as, diabetes, amyloidosis, hypertension, chronic obstructive pulmonary disease (COPD), and coronary heart diseases (Guan et al., 2020; Magadum & Kishore, 2020).

1.3.1 Pulmonary Morphological Stages of Coronavirus Disease

The pulmonary stage of Coronavirus disease is divided, into four morphological stages.

- Early stage (day 0-1)
- Exudative stage of diffuse alveolar damage (DAD) (day 1-7)
- Organizing stage (1-several weeks)
- Fibrotic stage of DAD (weeks-months)

1.4 Diagnosis of CoV-19

Covid-19 can be investigated by performing various tests. PCR is considered a gold standard technique to diagnose Covid-19 infections (Falzone et al., 2021). Low sensitivity is one of the major reasons that limits real-time PCR (RT-PCR), and incorrectly diagnosed samples with minimal viral load (Pan et al., 2020). However, false-positive, or false-negative results lead to several limitations and criticisms, thus affecting prompt diagnosis and correct patient management (Fang et al., 2020). Other limitations include sample contamination and prolonged execution time for analysis. The first imaging technique for diagnosis of coronavirus is a chest X-ray. It is represented as ground-glass opacities (GGO), with basal, peripheral, and bilateral distribution (Abbas et al., 2020). The sensitivity of chest radiography has been limited for Covid-19, during an early stage of infection therefore, it is not recommended as a first-line imaging modality however, it is cheap and easily available (Zu et al., 2020). Covid-19 patients at early 2-4 days showed no image abnormalities on chest x-ray (Wong et al., 2020).

Prompt decision-making to isolate and treat Covid-19 infected patients can be supported by non-contrast thoracic computerized tomography (CT) scans. CT images represent infected lung as Ground Glass Opacity (GGO), crazy paving, and consolidation (Li et al., 2020). Multiple CT slices give detailed information about the damaged lung. The equipment is not easily available in various hospitals and is also not cost-effective. High-resolution computerized tomography (HRCT) is considered a preferred method of diagnosis because it provides a clear image of the tiny structure of lung tissues (Shah et al., 2021). The overall sensitivity of HRCT is higher and is proven as a standard imaging method that can access the progression and severity of disease (Shah et al., 2021). However, it is important to identify patient's timely who may become critically ill, for subsequent active interventions. It is necessary to consider patient triage, and designing the treatment protocols, and performing follow-up evaluations for the improvement of clinical outcomes.

1.5 Role of Deep Learning (DL) in the Diagnosis of Coronavirus

In recent years, DL one of the major sub-filed of Artificial Intelligence (AI), has played a central role in medical image analysis (Shin et al., 2016). DL has proposed a potential method that used CT images for identification of diffused lung diseases. In contrast to a traditional visual evaluation of CT scans, DL is more effective in automatic image classification tasks. In DL, one of the most prominent and important models is CNN which in many application areas has shown its advantages, such as in medical diagnosis, speech recognition, and computer vision (Shin et al., 2016). LeCun proposed a special neural network called convolution neural network (CNN) used for image recognition that made a great breakthrough in target detection (Girshick et al., 2016), images retrieval and classification (Krizhevsky et al., 2017).

There is an increase in number of hidden layers (convolution and sampling layer) in deep CNN, and the image dimension has been reduced which in low dimensional space extracts sparse image features. It is easier to train because weight-sharing CNN has few parameters and neurons. CNN have been proposed as potential solutions to identify damaged lung of a person with pulmonary disease, by distinguishing lung tissues from surrounding structures (Soni et al., 2022). A wide range of training skills and network settings have been

developed by Alex et al. including local response normalization, pooling, ReLU, and dropout. This is helpful for more effective training of deep CNN and gives better results (Rawat & Wang, 2017).

1.6 HRCT Dataset and Covid-19 Classification

This study uses five different pre-trained networks ResNet50V2, InceptionV3, Xception Net, EfficientNetB0, and MobileNetV2 on publicly available dataset, which is preprocessed (Rahimzadeh et al., 2021). The data augmentation technique is applied to attain diversity. The image classification performance of small data sets using CNN-based methods can be improved by adopting data augmentation. The data set has been loaded in batches and pre-trained weights of the ImageNet dataset have been used. The transfer learning technique has been applied, for achieving the best accuracy (Shin et al., 2016). After concatenating the last connection layer, the output comes as 0 for a normal image and 1 for a covid-19 infected image. Best checkpoints for each model are saved after training, which are then used for the evaluation of the proposed model. The accuracy, sensitivity, specificity, and precision values for all five models have been calculated. Furthermore, feature visualization algorithm investigated covid-19 infected and normal images by generating heat maps.

1.7 Research Aim and Objective

The basic aim of the study is to propose a fully automated model for an accurate and rapid detection of Covid-19 from HRCT images using deep learning. The implementation of deep learning frameworks in medical image classification is an important task. The basic objectives of the study are as under:

- Propose a light weight more accurate model that out-performs previously proposed models
- Compare different pre-trained DNN models in order to find the best optimized architecture
- Reduce the burden on radiologist by automatic and accurate detection of disease
- Objective diagnostic

CHAPTER 2

LITERATURE REVIEW

RELATED WORK

2.1 SARS-CoV-2

From the past 2 years, novel coronavirus SARS-CoV-2 greatly affected billions of people, globally. In December 2019, city of China, Wuhan 41 atypical pneumonia cases with unknown etiology (Huang et al., 2020). In early January 2020, there was rapid increase in number of atypical pneumonia in Wuhan which began spreading across China and other countries (Nishiura et al., 2020).

Iranian Health Authorities from February 19 up to March 9, 2022, officially reported surveillance cases data to estimate incidence rate of confirmed infections (Arab-Mazar et al., 2020). It affected 1.2 billion people globally and up to March 2021 causing >2.7 million deaths (2020). Patients aged >65 years with Covid-19 to be found 6 times higher mortality as compared to younger (Wu et al., 2020).

2.2 Mechanism of Invasion of SARS-CoV-2 into Host Cell

Coronaviruses are single-stranded RNA viruses, of approximately 30kb which are enveloped and can infect a variety of host species (Channappanavar et al., 2014). Based on the genomic structure, they are further divided into four genera: α, β, γ, and δ, of which only two of them α, β can infect mammals (Rabi et al., 2020). Common cold and croup caused by 229E and NL63 human coronavirus. However, β coronaviruses are responsible for Severe acute Respiratory Syndrome Coronavirus (SARS-CoV), Middle East Respiratory Syndrome Coronavirus (MERS-CoV), and Severe Acute Respiratory Syndrome Corona Virus-2 (SARS-CoV-2) which causes COVID-19.

There are 5 steps involved in life cycle of virus: initial attachment with host, penetration, after that biosynthesis, then maturation and finally release. Viral attachment occurs when it binds to the host receptors. In penetration, by process of membrane fusion or endocytosis viruses enter the host cells. Viral RNA for replication entered nucleus, and inside host cells releasing viral contents. In the third step biosynthesis, new viral proteins are made up of viral mRNA. Finally, new viral particles are synthesized, matured, and then released.

2.2.1 Structure of Coronavirus

Four structural proteins are involved in the composition of coronavirus: (i) Spike (S), (ii) Membrane (M), (iii) Envelop (E), and nucleocapsid (N) (Bosch et al., 2003). Diversity of host tropism with coronaviruses is determined by spike. Trimetric transmembrane glycoprotein is involved in the composition of spike which protrudes from surface of virus. Two functional subunits S_1 and S_2 co spike, and S_1 unit is for viral binding to host cell receptor and S_2 subunit is responsible for cellular membrane fusion with viruses. For SARS-CoV, Angiotensin-converting enzyme-2 are considered as functional receptors (ACE2) (Li et al., 2003).

ACE2 and SARS-CoV spike bound have been reported through functional and structural analysis (Letko et al., 2020; Chen et al., 2020). In lungs, kidney, heart, bladder, and ileum ACE2 expression is remarkably high (Shu et al., 2020). Lungs epithelial cells highly expressed ACE2. However, further investigation is still needed whether SARS-CoV binds to an additional target or not. Protease cleavage occurs in spike protein, when SARS-CoV-2 binds with host protein. To activate protein spike of MERS-CoV and SARS-CoV two sequential protease cleavage was proposed as a model. It consists of cleavage at S_1 and S_2 sites for priming, and cleavage at S_2 site for activation, within S_2 subunit an adjacent position to fusion peptide (Ou et al., 2020; Belouzard et al., 2009; Millet & Whittaker, 2014).

Non-covalent binding remains in S_1 and S_2 subunits after cleavage at S1/S2 cleavage site, while to stabilize the membrane-anchored and pre-fusion state the distal S1 subunit and S2 subunit contributes, respectively (Walls et al., 2020). Spike for membrane fusion activates due to subsequent cleavage at S2 site, through some irreversible conformational changes. As different proteases cleave and activate it so, spike of coronavirus is unusual (Belouzard et al., 2012). The existence of "RPPA" sequence (furin cleavage site) at S1/S2 site, characterized SARS-CoV-2 as unique among other coronaviruses. However, furin existence makes this virus more pathogenic.

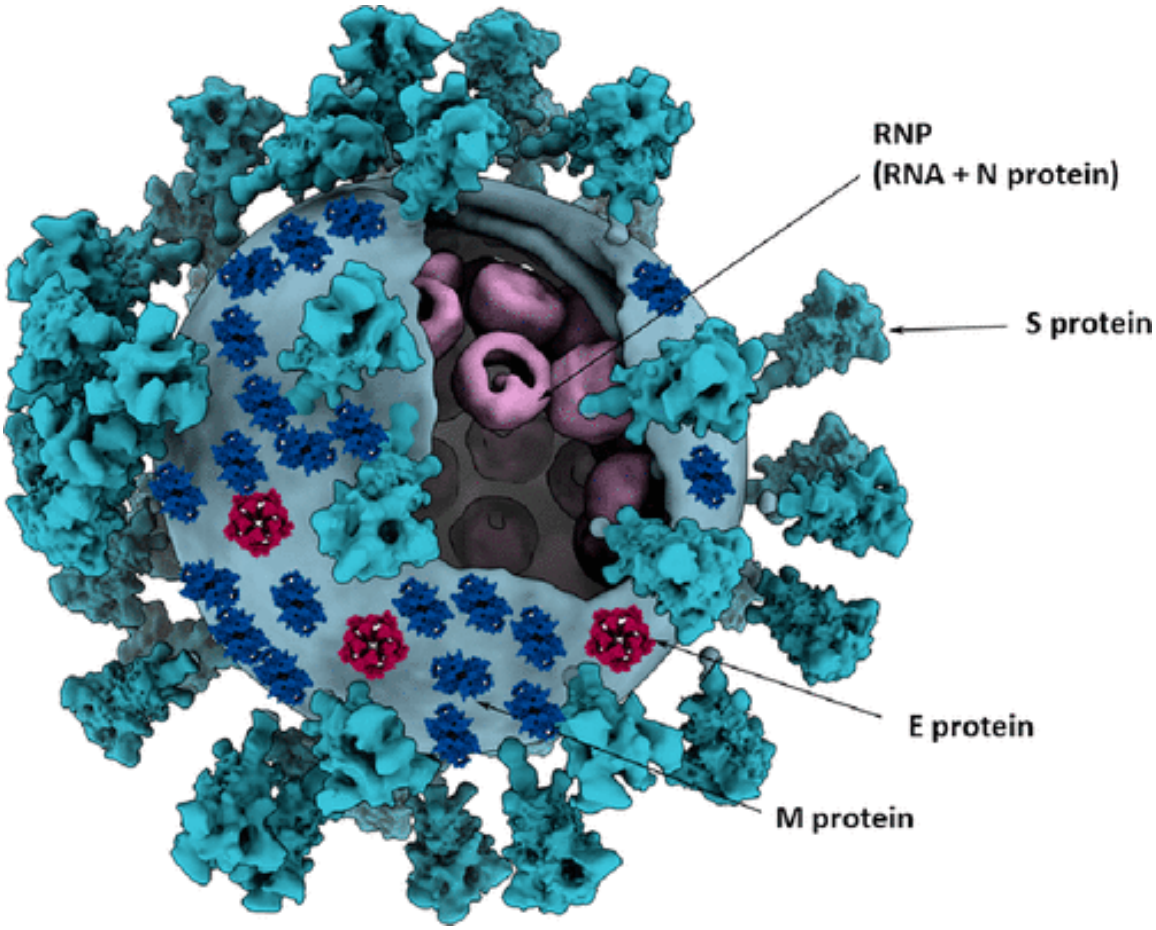

Figure 2: 3-Dimensional (3-D) Structure of SARS-CoV-2 showing: M (Membrane), S (Spike), E (Envelop), and N (Nucleocapsid) structural proteins (Saville et al., 2022)

2.3 Coronavirus Disease 2019 and Patient Classification

The coronavirus disease hits the patients differently and classified them as symptomatic and asymptomatic. In symptomatic patients, clinical presentations may vary from patient to patient and are sub-divided in to mild, moderate, and severe cases (Ruan et al., 2020; Mahase, 2020; Wu & McGoogan, 2020). However, asymptomatic patients usually do not show any sign and symptoms. The classification of symptomatic and asymptomatic patients is described in Table 1.

Table 1: Symptomatic and Asymptomatic Classification of Patients with Coronavirus Disease

Classification	Clinical Presentations
Asymptomatic	No clinical sign and symptoms, but COVID test positive and normal chest imaging
Symptomatic Mild	Acute upper RTI (respiratory tract infection) symptoms such as cough, fever, sneezing, sore throat, myalgia, fatigue, or digestive symptoms like abdominal pain, diarrhea, nausea, and vomiting
Symptomatic Moderate	Frequent fever and cough, pneumonia-like symptoms chest CT with lesions but no obvious hypoxemia
Symptomatic Severe	Pneumonia along with hypoxemia, SPO2 is less than 92%
Symptomatic Critical	ARDS, heart failure, myocardial injury, may have shock, coagulation dysfunction, acute kidney failure, or encephalopathy

2.4 Medical Image Classification

Medical image classification plays an important role in teaching tasks and clinical treatments. To label and collect medical image datasets, a lot of professional expertise is required. For different classification tasks, Machine Learning (ML) methods are available. The deep neural network (DNN) is one of the emerging ML methods. The best results of image classification tasks can be achieved by CNN (Chaudhary et al., 2021; Rahimzadeh et al., 2021).

2.5 Machine Learning and Image Classification

Martinez et al., (2021) used machine learning approach for an early detection of coronavirus disease exclusively based on self-reported symptoms. The area under the curve for receiver operating characteristic (AUC), specificity, and sensitivity showed 72.8%, 60.9%, and 75.2%, respectively (Martinez-Velazquez et al., 2021).

Han et al., (2021) used symptoms and voice signals combination of covid-19 infected patients while recording coughing audios. Author processed data training using Support Vector machine (SVM) and reported specificity and sensitivity of 82% and 68%, respectively (Han et al., 2021).

Federico et al., (2020) develop, evaluate, and validate ML models using routine blood tests for the detection of coronavirus disease. Study used three different datasets and developed five ML models and achieved AUC from 75% to 78% and specificity ranges from 92%-96% (Federico et al., 2020).

Arpaci et al., (2021) considered fourteen different clinical features to predict coronavirus infection by implementation of ML classification algorithms. Author used six different classifiers for the development of six predictive models to diagnose corona virus disease. Results showed that CR-meta classifier is 84.21% accurate and could be helpful for the diagnosis of disease (Arpaci et al., 2021).

2.6 Deep Learning and Image Classification

The reliable and efficient medical imaging diagnosis can be achieved by the implementation of deep learning-based algorithms. In recent years, for the prognosis of pneumonia competitive sensitivity has been demonstrated by deep learning-based analysis using CT-scan.

Xue et al., used transfer learning technique for the classification of chest CT-scans to diagnose Covid-19. A novel pre-processing method have been used to classify volumetric CT scans by exploiting 3D Network-based transfer learning technique. The backbone network used in study was a pre-trained 3D ResNet50, trained on pneumonia, covid-19 infected and normal images. The results showed 82.86% covid-19 sensitivity and 85.56% overall accuracy (Xue & Abhayaratne, 2021).

Rahimzadeh et al., (2021) proposed highly accurate and rapid model for detection of Covid-19, from HRCT images. Image pre-processing algorithm was implemented to discard close lung images and then novel CNN architecture was designed to improve image classification. ResNet50V2 used as a backbone with feature pyramid network and achieved an overall accuracy of 98.49%. the overall accuracy on Xception Net was 96.55% with 98.02% covid-19 sensitivity (Rahimzadeh et al., 2021).

Anwar & Zakir (2020) used CT-scan images for the diagnosis of coronavirus disease 2019, by implementation of deep learning techniques. Efficient Net DL architecture has been used for rapid and accurate detection of disease. This study used three different learning strategies such as constant learning rate, cyclic learning rate, and reducing learning rate. The results showed an overall accuracy of 89.7%, F1 score 89.6%, an AUC 89.5% (Anwar & Zakir, 2020).

Chaudhary et al., (2021) proposed a CNN based classification architecture, for the detection of pneumonia and Covid-19 using CT-scan images. Initially, pre-trained Dense Net architecture has been used then applied Efficient Net for a fine-grained three-way classification. The results showed an overall accuracy of 90%, with 85.7% and 94.2% sensitivity for Covid-19 and pneumonia, respectively (Chaudhary et al., 2021).

Shamsi et al., (2021) motivated by medical diagnostics shortcomings and presented a framework for early and rapid detection of coronavirus disease 2019. Author used four different pre-trained networks such as ResNet50, InceptionResNetV2, DenseNet121, and VGG16 to extract deep features from CT-scan and chest X-ray images. The best results achieved which showed that estimated predictivity is much higher in CT-scans as compared to chest X-ray images (Shamsi et al., 2021).

2.7 Five Pre-trained Models

Literature showed that many authors used different models for medical image classification. Studies revealed that using DL for diagnosis of Covid-19 in image classification tasks, residual neural network (Res Net) (2D or 3D) has often been used, as a novel CNN architecture (Loey et al., 2020). ResNet was proposed as a novel CNN architecture in 2015 (He et al., 2016). ResNet inserts shortcut connections between layers after realizing identity mapping, which improves the CNN classification performance by adding new residual blocks after defining the function complexity.

The modified version of Res Net 50 is ResNet50V2, which on the ImageNet dataset performs better than ResNet101 and ResNet50 (Kondu et al., 2022; Rahimzadeh & Attar, 2020). A modification was made in ResNet50V2 between blocks, in the propagation formulation of connections. In 2017, the first version of Mobile Net was proposed that improves training efficiency of CNNs by reducing computational budget without compromising accuracy. It uses depth-wise separable convolutions, and builds lightweight deep neural networks (Howard et al., 2017).

Inception V3, third edition of Google's Inception CNN has been used for assisting object detection and image analysis (Szegedy et al., 2016). Initially, it was introduced during the ImageNet Recognition Challenge. Chollet was inspired by Inception and proposed a novel CNN architecture called Xception that contains depth-wise separable convolutions instead of inception modules (Chollet, 2017). In 2019, the most powerful CNN model proposed by Tan and Le named Efficient Net achieved 98.8% accuracy (Tan et al., 2019). The Res Net (Rahimzadeh et al., 2021), Mobile Net (Ahsan et al., 2021), Inception (Yamin et al., 2021), and Efficient Net (Shamila Ebenezer et al., 2022) showed effectiveness in detection of Covid-19 with an accuracy of 98.4%, 95%, 99%, and 94.5% respectively.

This study classifies the normal and covid-19 infected person as 0 and 1, by the implementation of CNN on the HRCT data set. In this work, the method involved is based on image classification that can detect the disease more accurately and rapidly, leading to better therapeutic interventions and management.

CHAPTER 3

MATERIALS & METHODS

MATERIALS and METHODS

3.1 Data Set

This study uses an open-source data set for training, validation, and to evaluate the proposed networks (Rahimzadeh et al., 2021). This three-dimensional (3-D) High Resonance Computerized Tomography (HRCT) image data set was acquired from the Negin radiology center, at Sari in Iran. To capture and visualize lung HRCT images from patients, the Negin center uses the syngo CT VG30-easyIQ software version along with the SOMATOM Scope Model. All 3-D images were converted into 2-dimensional images. It contains 48,260 CT images from 282 normal persons, and 15,589 images from 95 corona positive patients. Each CT scan has a volume of 512*512-pixel resolution in a grayscale 16-bit DICOM format. The patient's confidential information was excluded by converting DICOM format into TIFF, while maintaining the same 16-bit grayscale image.

Good predictive models divided the data set into three parts: for model fitting into the training set, the selection of the model into validation set, and for final assessment of model into the test set. In this study, dataset used in training contains 18676 images and 4000 images in validation set. To triangulate the proposed model, separate 4000 images in the test set were used. The data set has been divided into a 70:15:15 ratio with 18676, 4000, and 4000 images in training, validation, and testing folders, respectively. Pre-processing of a dataset has been done to make it amenable for training and model validation. The 16-bit image format improves our classification results as compared to 8-bit format that may cause to lose some data, particularly when there is a minimal lung infection.

The 16-bit CT scan image information is not visible to the naked eye; however, a computer can easily distinguish those images during processing. By considering maximum pixel value, scaling of each image can make covid-19 infectious image clearer. Standardized monitors can visualize 32-bit float-type, pixel values. It can be obtained as an output while dividing each image's pixel value, by the maximum pixel value of that image and then converting them into float. The output image for analysis is of good quality. In the experiments, the data set other than the above-mentioned is not used in our research because

we don't have many computational resources for such a large CT-scan data set. This section describes the datasets used in this research for training and testing.

3.2 Methodology

The generalized classification framework research is described below in this section. Five different pre-trained classification networks ResNet50V2, MobileNetV2, EffecientNetB0, InceptionV3, and XceptionNet have been used to achieve better performance by adjusting trainable parameters. A 2-Dimensional CT scan lung image with Ground Glass Opacity (GGO), crazy paving, or consolidation is considered as an input to investigate presence of suspicious patches by using proposed algorithm. Output classified the image and calculated the accuracy of the proposed model. This section includes a pipeline for an accurate image classification along with the details of network architecture. The schematic approach to image classification is shown in Figure 3.

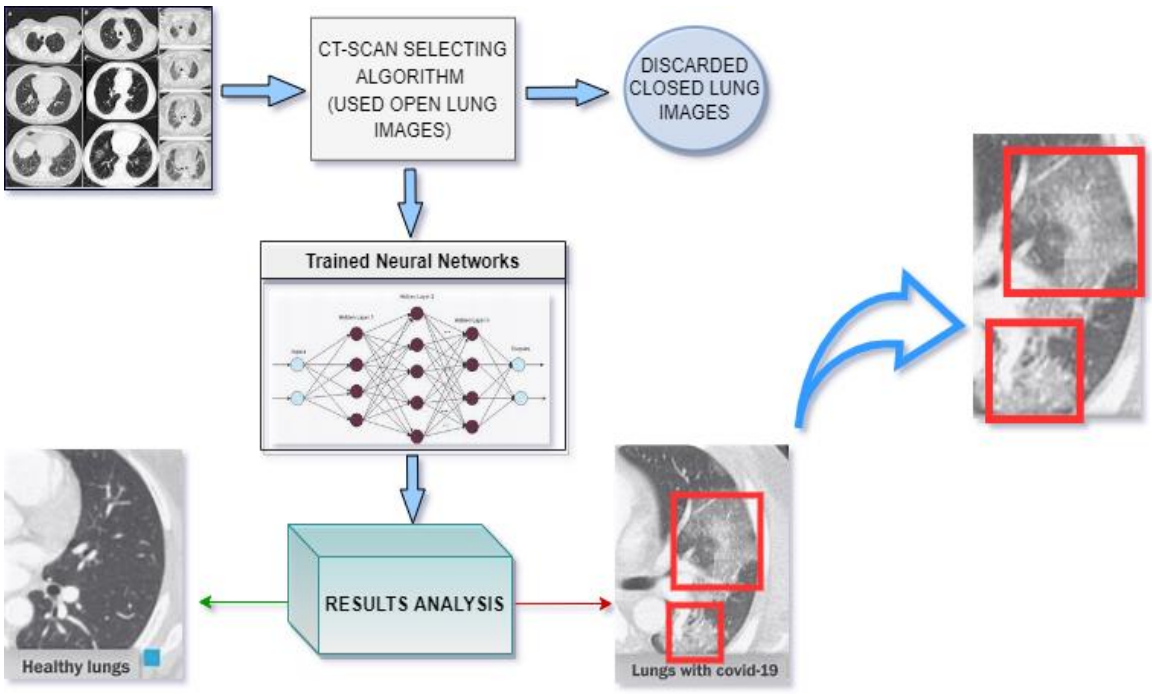

Figure 3: Schematic of image classification model trained on input CT scan images classifying normal and Covid-19 infected images

3.2.1 Pre-processing

The good generalization ability of the model can be achieved by splitting data sets into training, validation, and test set that significantly affects the model performance. Healthy CT images were more as compared to Covid-19 affected images. Here, at this point data set was split and training data set was divided with an equal number of infected vis-a-vis normal images.

3.2.1.1 CT -Scan Image Selection Algorithm

The consecutive sequence of images as taken by HRCT device contains multiple images in which the lung is not clear as shown in Figure 4. It would be difficult for a machine to evaluate Covid-19 infectious patients from a closed lung image. Moreover, these images become a burden on computational resources and slow down training process. Hence, unclear lung images were discarded using image selection algorithm.

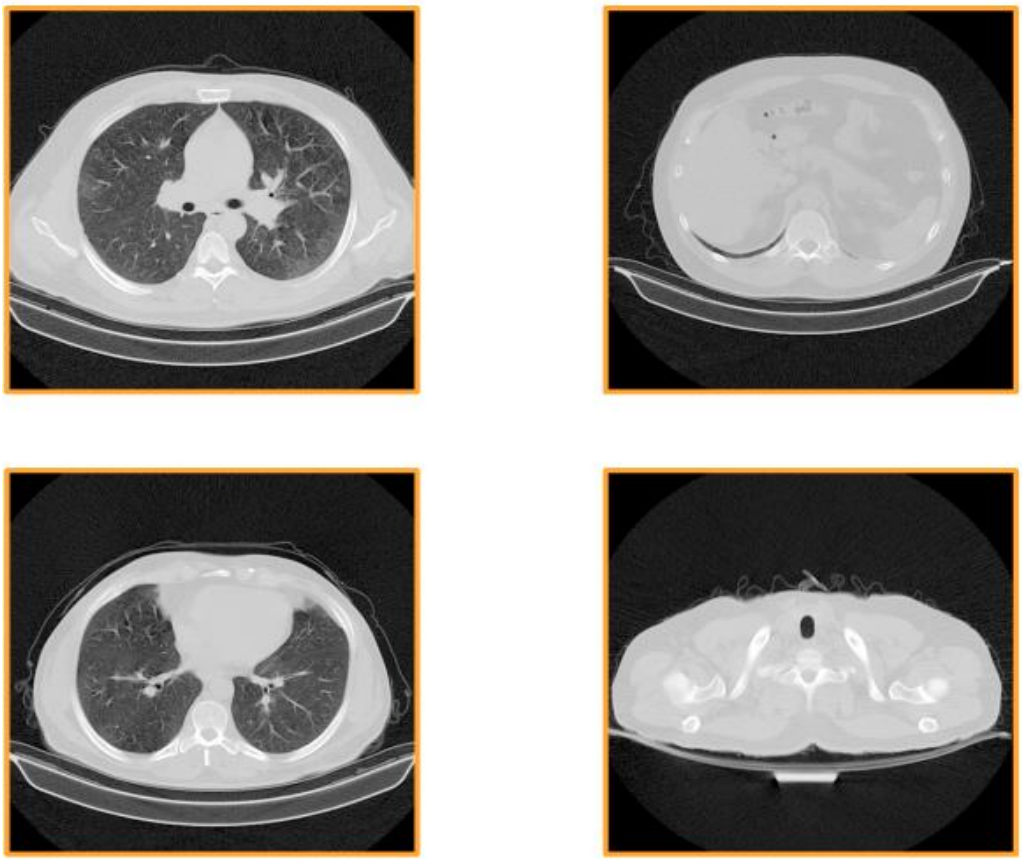

Figure 4: Open lung image (left) close lung image (right)

Each CT scan image sequence contained a close lung image at its beginning and end as shown in Figure 5. Open and closed lung has a clear difference in this centralized area. Algorithm discarded close lung images and considered only middle sequence of lung images, with lower pixel values (near to black).

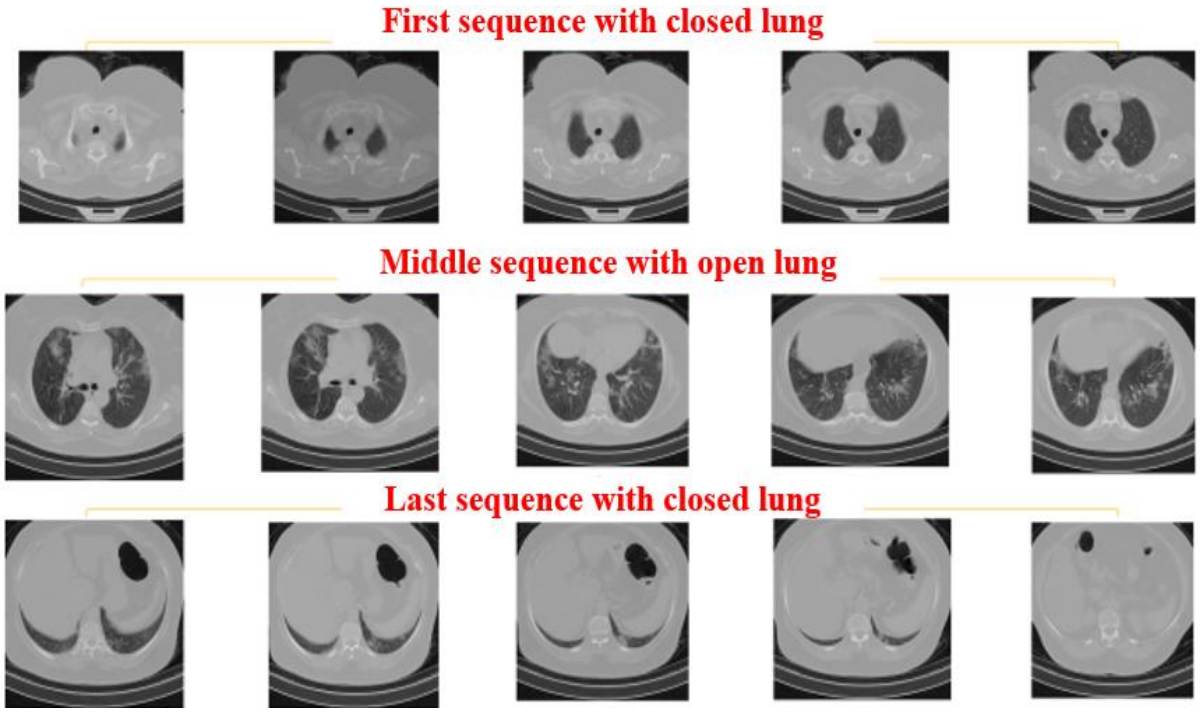

Figure 5: First, middle, and last sequence of CT-scan image of lungs. First and last sequence shows closed lung image

In an image of 512*512*1--pixel resolution specific region was selected because patient's position was different from one another while performing HRCT scan. This central area covers 120-370 pixels on x-axis and 240-340 pixels on y-axis. In all images, the middle area of the lung between these pixel values, 120,240 and 370,340, will justify whether it is an open or close lung image, by calculating lower or higher pixel values. Maximum pixel values in all images are almost approximately equal to 5000 but may differ in some cases. Any image with a value less than 300 is considered a dark pixel and discarded.

3.2.2 Data Augmentation

To make it more heterogeneous and diverse, data augmentation was applied to training dataset. Before applying different augmentation options, it is necessary to make the model

more generalized with respect to images. Horizontal and vertical shift and zoom ranges with a 20% probability were added. Similarly, if an image in the test set is rotated at a certain angle, the model will struggle to give desired prediction. A rotation range of 360 degrees can be useful to overcome this problem. It was observed that at certain times, images changed their height and width during the process. This problem was addressed by adding height and width shifts with a 20% probability. To capture shear features shear range was added in the images, applied with 3% probability. Augmentation of randomized normal and infected images shown in Figure 6 and data augmentation parameters are illustrated in Table 2.

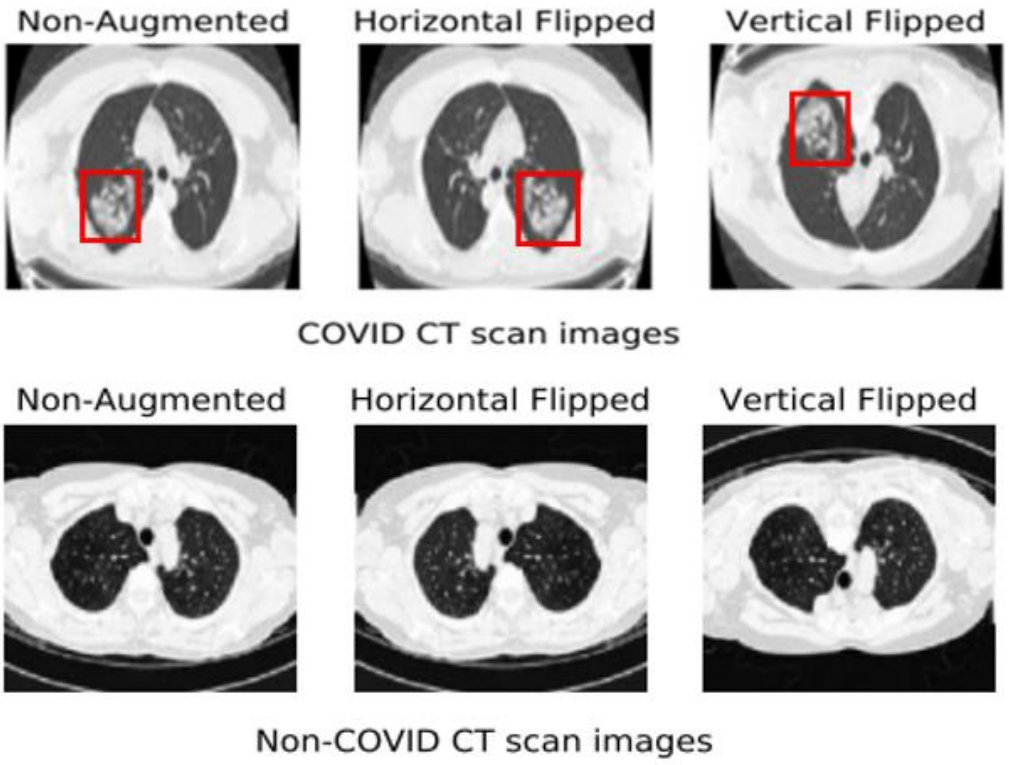

Figure 6: Randomized augmented and non-augmented infected and normal images

Table 2: Data Augmentation Parameters

Data Augmentation options	**Value**
Horizontal Flip	True
Vertical Flip	True
Rotation Range	360º
Zoom Range	0.2
Shear Range	0.03
Height Shift Range	0.2
Width Shift Range	0.2

3.2.3 Network Architecture

Since 2012, a significant performance in image classification tasks has been achieved by using DNN, more specifically CNN (Rawat et al., 2017). The proposed algorithms take CT scan images as input while extracting the important features and relevant information resulting in binary classification. Figure 2 Illustrates overall framework of design. and relevant information resulting in binary classification. Figure 7 Illustrates overall framework of design.

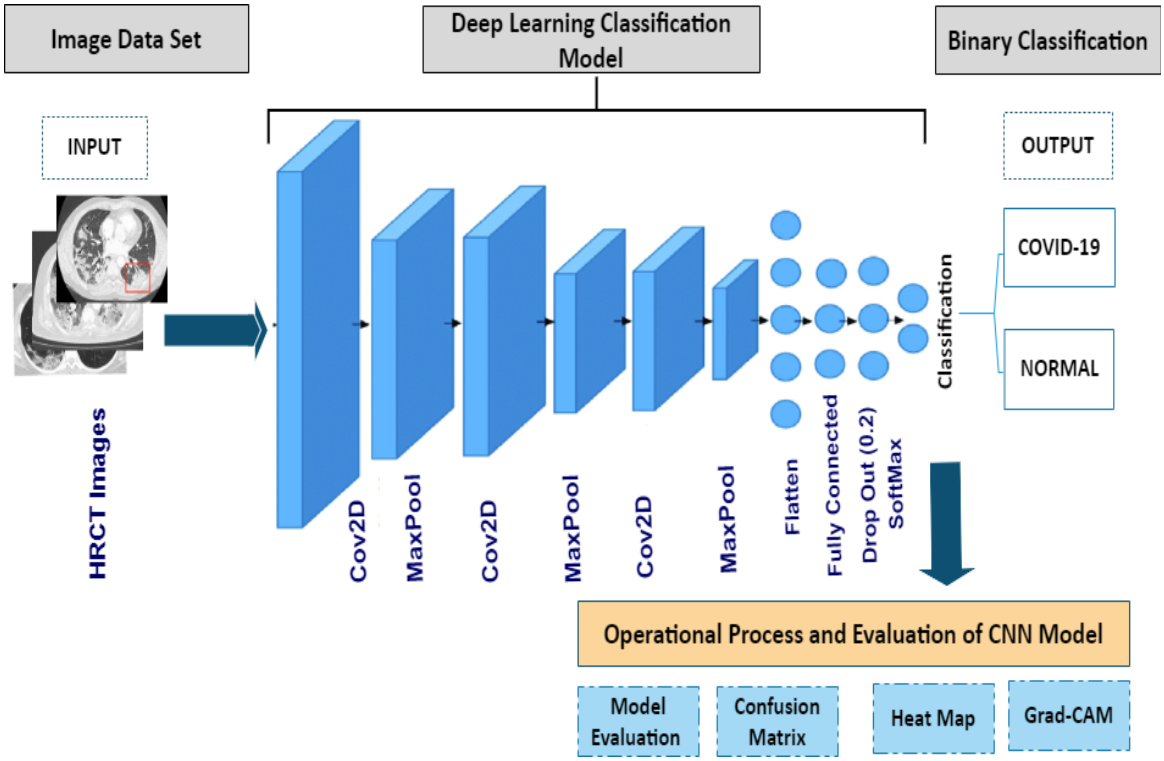

Figure 7: Network Architecture of the Proposed CNN Model

The first layer is convolution layer, number of parameters to be learned is reduced in simple network architecture that helps to avoid model over-fitting. In model learning, CNN combines weights into smaller kernel filters. The second layer is pooling layer followed by flattened layer and fully connected layer. Pooling layer plays a significant role for feature dimension reduction in CNN. Output neurons are reduced in convolution layers, while neighboring elements in convolution output matrices can be reduced by max-pooling. The pooling layer selects highest values from neighboring elements of input matrix and generates one element output matrix. This research uses transfer learning technique (Shin

et al., 2016). In each layer drop-out algorithm randomly disables neurons and improves model performance during training. The flatted layer, 0.2 drop value was added and concatenated last layer with an output of 0 and 1. After evaluating the proposed networks, the overall accuracy gives the authenticity of the model.

3.2.4 Training

The data was loaded into batches for training, data generators were applied for training, validation, and test sets. Five different deep learning pre-trained models, ResNet50V2, InceptionV3, Xception Net, EfficientNetB0, and MobileNetV2 were selected. For each model pre-trained weights on ImageNet dataset were used, that had been trained on 1.2 million images of 1000 classes. Since images in our dataset have (512, 512, 1) shape, however, models have been trained on ImageNet dataset with three channels. Here, any mismatch can be skipped in first layer. The hyper parameters are demonstrated below in Table 3.

Table 3: Training Hyperparameters

Hyper-parameters Name	Value
Learning Rate	1e-4
Number of Epochs	15
Dropout	0.2
Batch size	16

Each model adds a dropout value of 0.2 that switched off 20% of neurons in second last layer in the network. Furthermore, last classification layer was customized there are only two outputs 0 and 1 for normal and covid infected classification. Since the dataset was large, it was necessary to fine-tune each model to update parameters. During the training of each model, categorical cross-entropy loss and Adam optimizer were used.

Our model training selected a batch size of 16 for 15 epochs. EfficientNetB0 outperformed all other models with a training accuracy of 99.6%. For each iteration different data has been introduced to the network because several data augmentation schemes are already applied to dataset during runtime. This increases overall accuracy of the model by preventing overfitting.

3.2.5 Evaluation

After training, best checkpoints for each model were obtained, the evaluation of the model can be performed by loading the best checkpoints. The evaluation data set had 4000 mixed images of covid-19 infected as well as from normal subjects. In this stage, COVID sensitivity and specificity, normal sensitivity and specificity, accuracies and precision of infected and normal cases had been calculated for each model.

3.2.5.1 Evaluation Parameters

Certain parameters are used to measure model performance and accuracy however, the following matrixes are very important for evaluation. Evaluation parameters as demonstrated in Table 4.

Table 4: Evaluation Parameters

Evaluation Parameters	Description
True Positive (TP)	Infected and results identified it correctly as an infected image
True Negative (TN)	Normal and results showed it normal image
False Positive (FP)	Normal but results indicated it as diseased one
False Negative (FN)	Infected but result showed it as normal

3.2.5.1.1 Accuracy

The classification models can be evaluated by using an accuracy metric. To confirm that our model got right, accuracy is considered as the fraction of predictions. The accuracy can be calculated by considering some correct predictions and dividing them by a total number of predictions (Jin Huang & Ling, 2005). In binary classification networks, we can calculate the accuracy of the proposed model in terms of positives and negatives as follows:

$$Accuracy = \frac{True\ Positive + True\ Negative}{True\ Positive + False\ Positive + True\ Negative + False\ Negative}$$

$$Accuracy = \frac{TP + TN}{TP + FP + TN + FN}$$

3.2.5.1.2 Sensitivity

Sensitivity refers to a condition that has the ability, to correctly identify diseased patients. This test is useful for the identification of serious but treatable diseases with higher sensitivity values. It is the probability of a positive test, truly being a positive condition.

$$Sensitivity = \frac{TP}{TP + FN}$$

The sensitivity of the model can be calculated by considering the number of true positive images, which is then divided by number of false negatives and true positives. The disease can be ruled out with high sensitivity if false-negative results are low (Altman & Bland, 1994; Parikh et al., 2008).

3.2.5.1.3 Specificity

The specificity has the ability, to correctly identified normal persons. It is the probability of being negative when the disease is absent. Test specificity can be obtained by considering the TN value, and then dividing by TN and FP values.

$$Specificity = \frac{TN}{TN + FP}$$

Specificity does not consider false negative values. High specificity with a positive result in a test is useful for ruling in disease. In healthy persons, specificity rarely gives a positive result. If the result is positive, it signifies the disease probability with a higher probability (Parikh et al., 2008).

3.2.5.1.4 Precision

Precision is the value that conveyed an amount of information. It can be calculated by taking true positive values, which are then divided by true positive and false positive values.

$$Precision = \frac{TP}{TP + FP}$$

Precision indicates the relevant percentage of results (Scott 1999).

3.2.6 Inference

The test set evaluation can be accomplished by using inference, which was measured by calculating the total time taken by the model on test set. Calculate the total time in minutes and then convert it into seconds and then divided it by the total number of test images. The model training is patch-based and to dataset size, we applied data augmentation techniques during training, thus increasing the network accuracy and robustness. Additionally, an independent test set was used to evaluate our model and a confusion matrix was generated of all five networks.

3.3 Study Framework

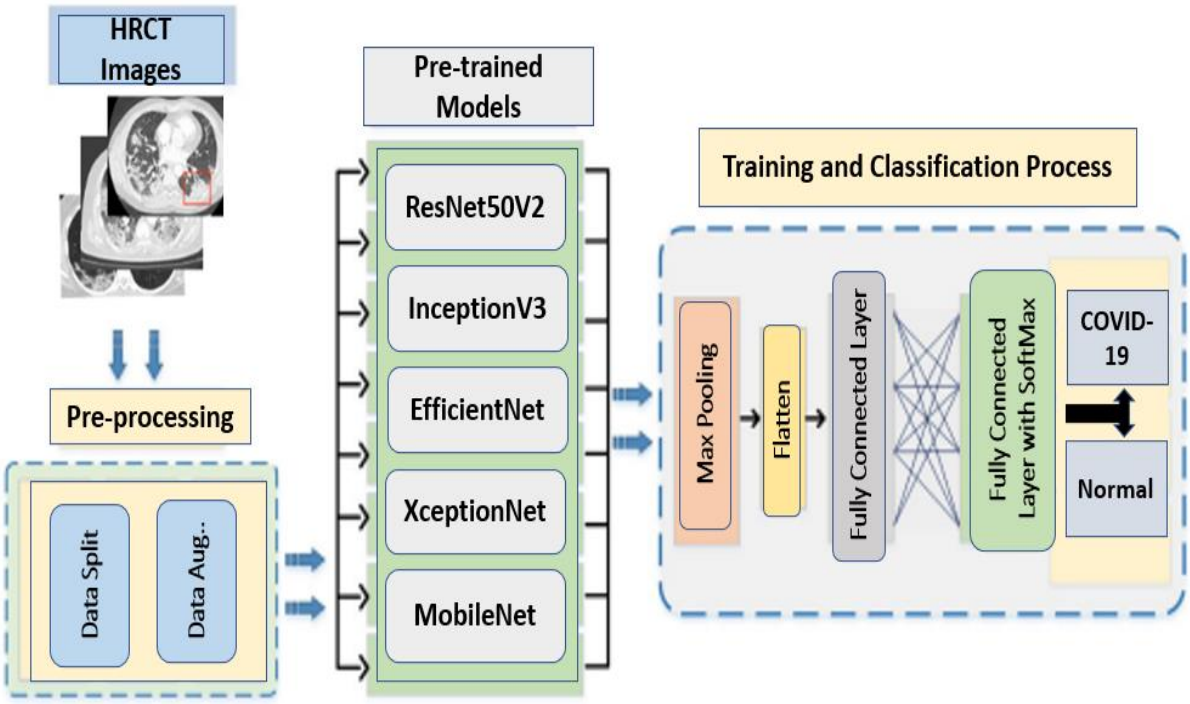

Figure 8: Overall study framework

CHAPTER 4

RESULTS

RESULTS

The network and algorithms were implemented by using Google Colaboratory (Google Colab) Notebooks. This research included five different deep learning models to classify the CT scan images and used Keras library to develop and run deep networks. The result section is further divided into two sub-sections. The first part involves the image classification results and second part covers patient condition that can be identified by adjusting the threshold 0.

4.1 Image Classification Results

The proposed network can differentiate between infected and non-infected classes as seen in Figure 8. The results of all five trained networks ResNet50V2, Inception V3, Xception, Efficient Net, and Mobile Net V2 on training and validation sets are represented in Figures 9, 10, 11, and 12. The comparison of all five algorithms and their respective accuracy and loss can be observed in Table 5 and 6. Loss curves are plotted for all five models, training procedure uses 15 epochs to show training and validation accuracy. Out of five networks EffecientNetB0 achieved the higher accuracy.

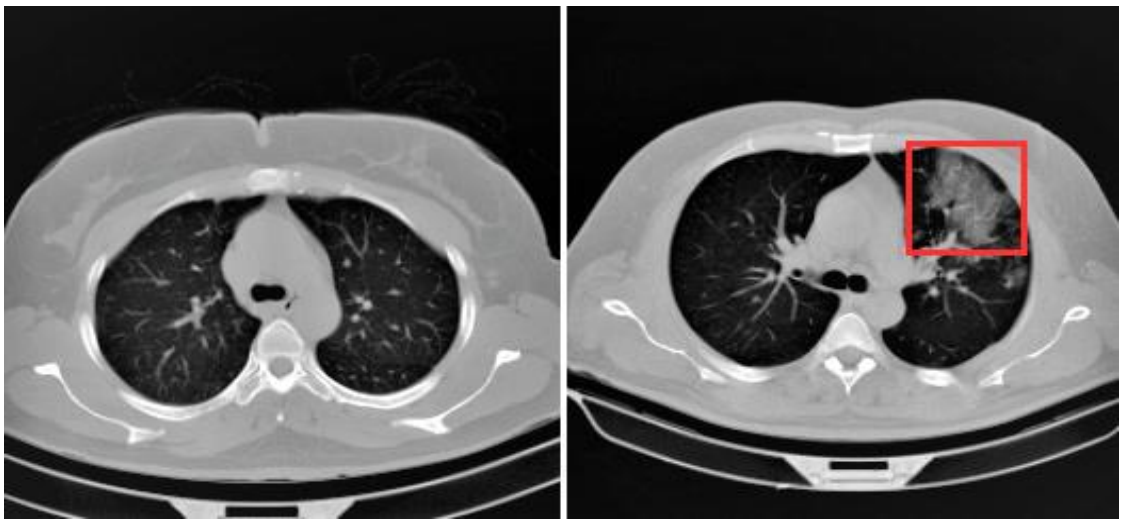

Figure 9: Classification of Normal (left) and infected (right) HRCT Image detected by the developed algorithm

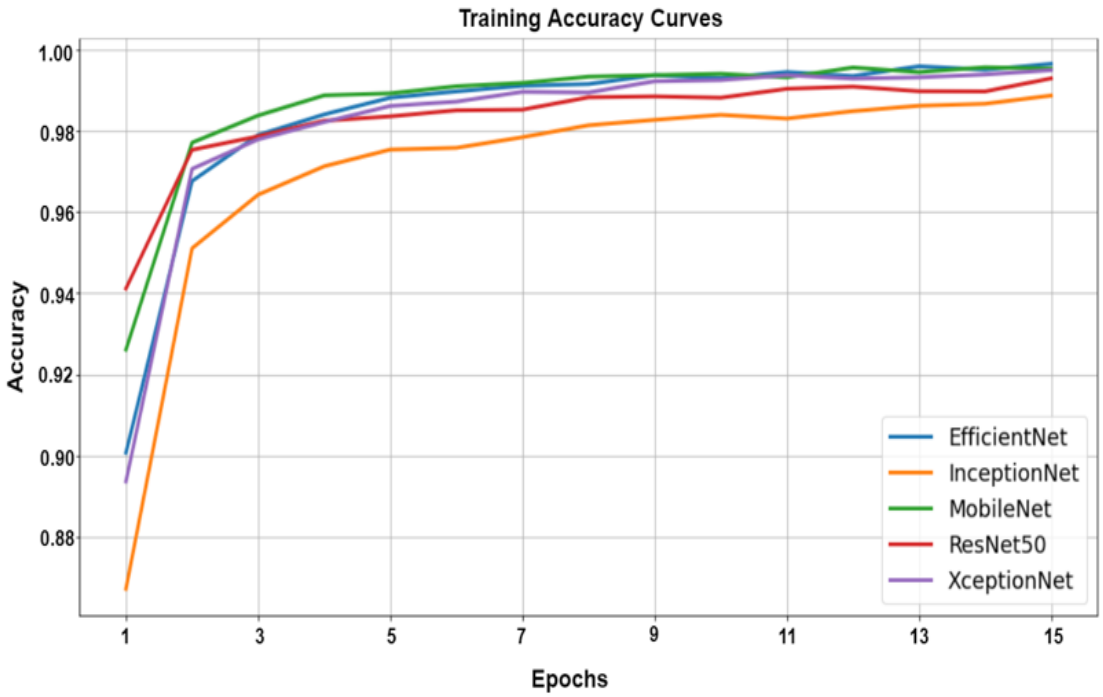

Figure 10: Training accuracy plot showing 15 epochs on x-axis and accuracy on y-axis

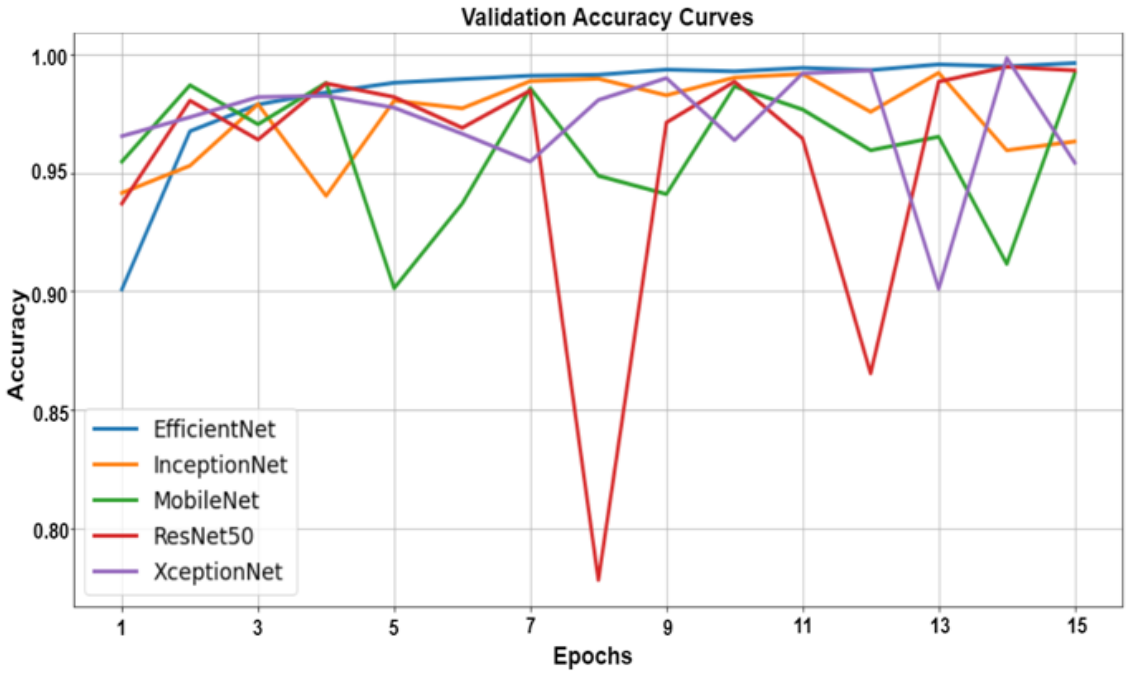

Figure 11: Validation accuracy plot showing 15 epochs on x-axis and accuracy on y-axis

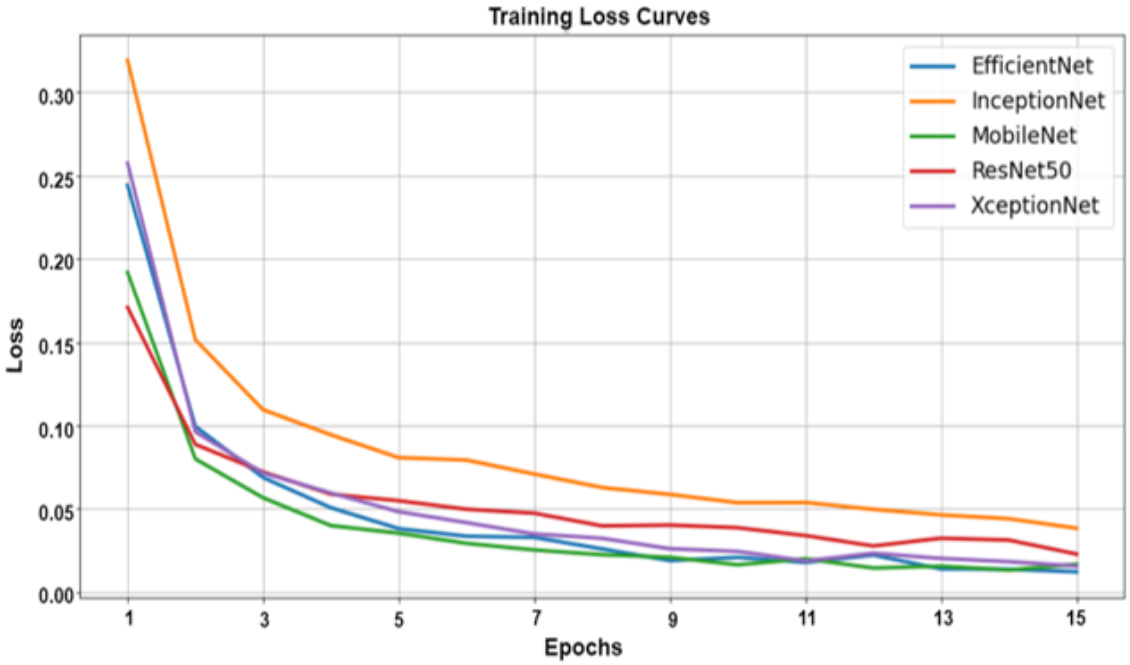

Figure 12: Training loss plots showing 15 epochs on x-axis and loss on y-axis

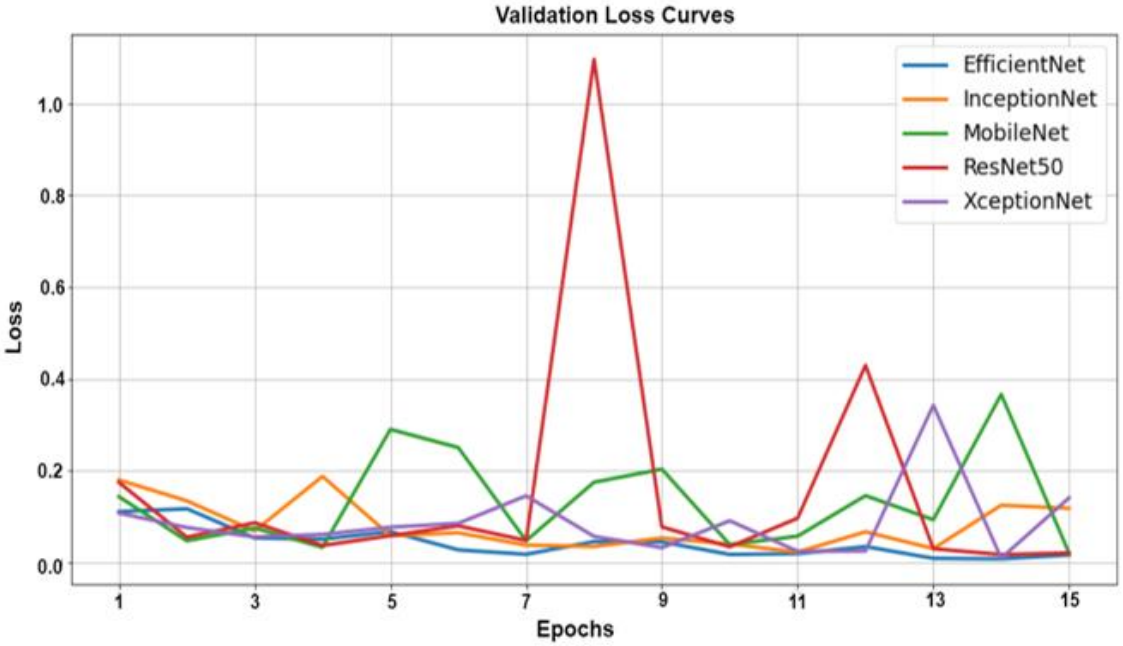

Figure 13: Validation loss plots showing 15 epochs on x-axis and loss on y-axis

Table 5: Training accuracy for 15 epochs

ResNet50V2	Inception V3	EffecientNetB0	XceptionNet	Mobile Net V2
0.9412	0.8673	0.9008	0.8050	0.9261
0.9752	0.9510	0.9676	0.8964	0.9770
0.9786	0.9642	0.9789	0.9374	0.9837
0.9824	0.9712	0.9839	0.9556	0.9886
0.9835	0.9753	0.9881	0.9640	0.9891
0.9850	0.9757	0.9896	0.9708	0.9909
0.9851	0.9783	0.9910	0.9745	0.9917
0.9882	0.9813	0.9914	0.9754	0.9932
0.9884	0.9826	0.9936	0.9793	0.9936
0.9881	0.9838	0.9929	0.9807	0.9939
0.9902	0.9829	0.9943	0.9827	0.9931
0.9908	0.9847	0.9934	0.9835	0.9955
0.9897	0.9861	0.9958	0.9839	0.9943
0.9896	0.9866	0.9949	0.9862	0.9955
0.9928	**0.9886**	**0.9964**	**0.9875**	**0.9952**

Table 6: Validation Accuracy for 15 Epochs

ResNet50V2	Inception V3	Efficient Net B0	Xception	MobileNetV2
0.9370	0.9415	0.9605	0.7660	0.9548
0.9805	0.9530	0.9553	0.9043	0.9870
0.9640	0.9790	0.9825	0.9218	0.9705
0.9877	0.9402	0.9837	0.9330	0.9880
0.9820	0.9805	0.9705	0.9517	0.9013
0.9690	0.9772	0.9923	0.9380	0.9370
0.9847	0.9887	0.9942	0.9690	0.9858
0.7780	0.9898	0.9815	0.9732	0.9488
0.9712	0.9827	0.9818	0.9682	0.9410
0.9885	0.9902	0.9952	0.9860	0.9865
0.9645	0.9918	0.9935	0.9578	0.9768
0.8652	0.9758	0.9885	0.9333	0.9595
0.9885	0.9923	0.9975	0.9868	0.9653
0.9948	0.9595	0.9873	0.9768	0.9115
0.9933	**0.9632**	**0.9937**	**0.9762**	**0.9920**

4.1.1 Model Evaluation

The accuracy metric has been used to find out the best training network to monitor validation results. To evaluate overall accuracy of all five networks four different matrices were used that classify infected and non-infected cases. Confusion matrices (CM) containing accuracy, specificity, sensitivity, and precision values for evaluation of each model is shown in Figures 13, 14, 15, 16, and 17.

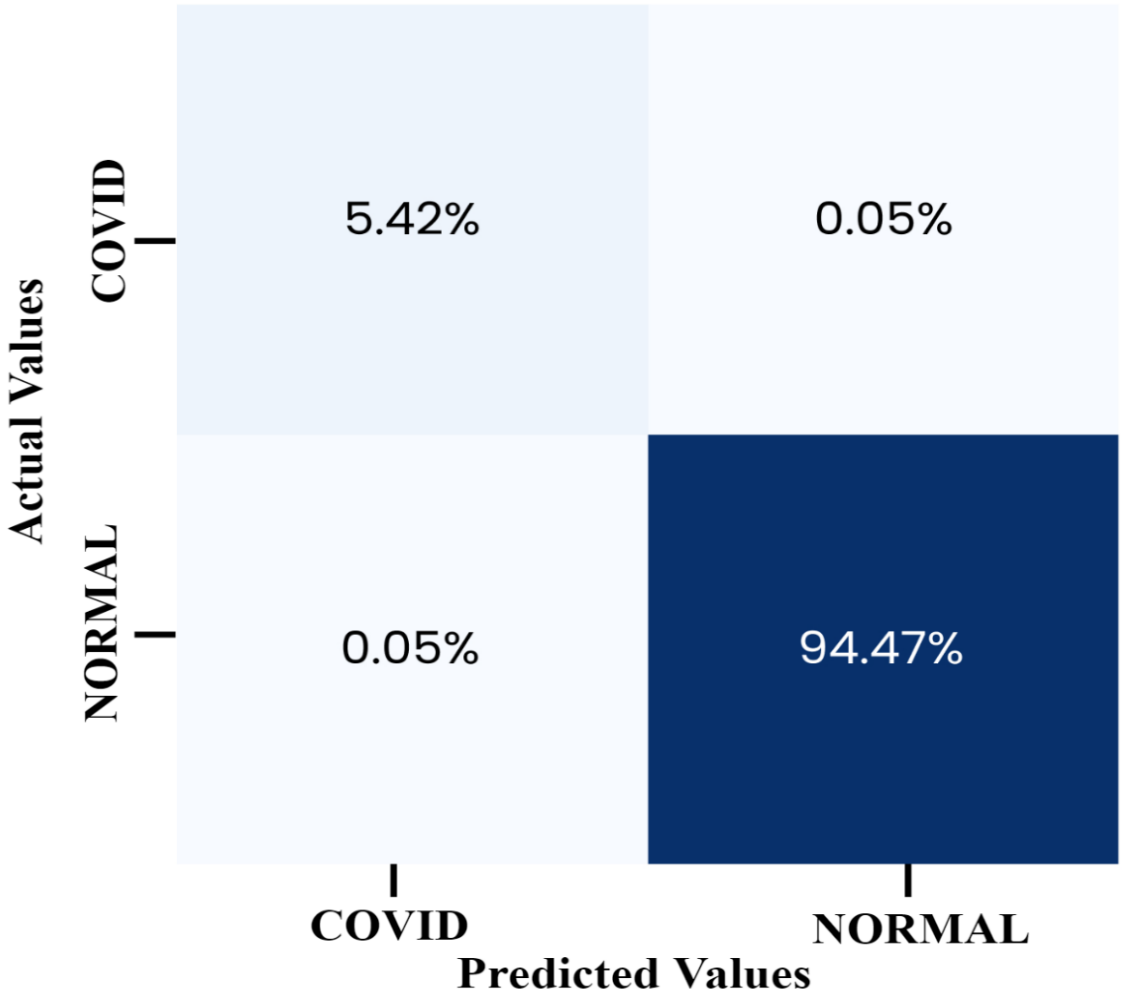

Figure 14: Confusion Matrix showing ResNet50V2 test evaluation

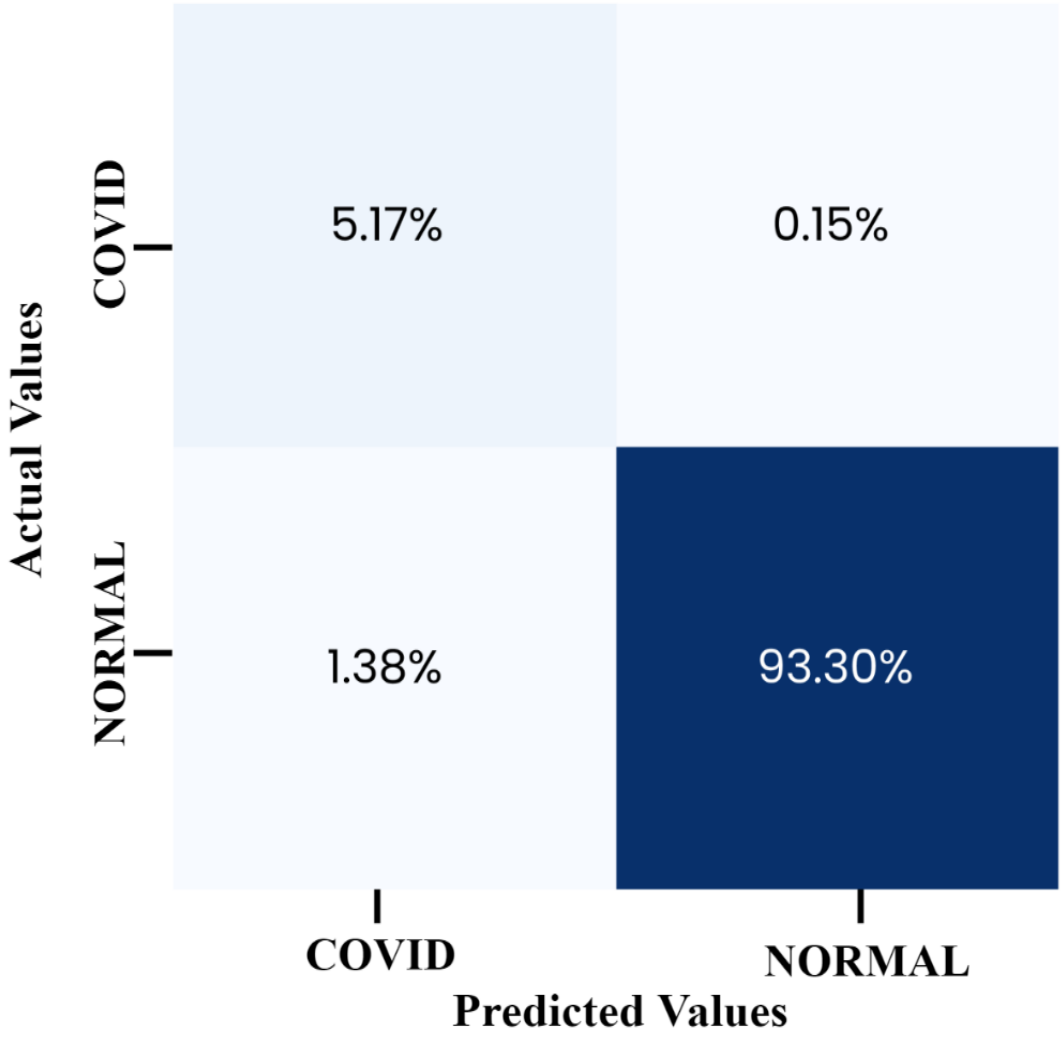

Figure 15: Confusion Matrix showing InceptionV3 test evaluation

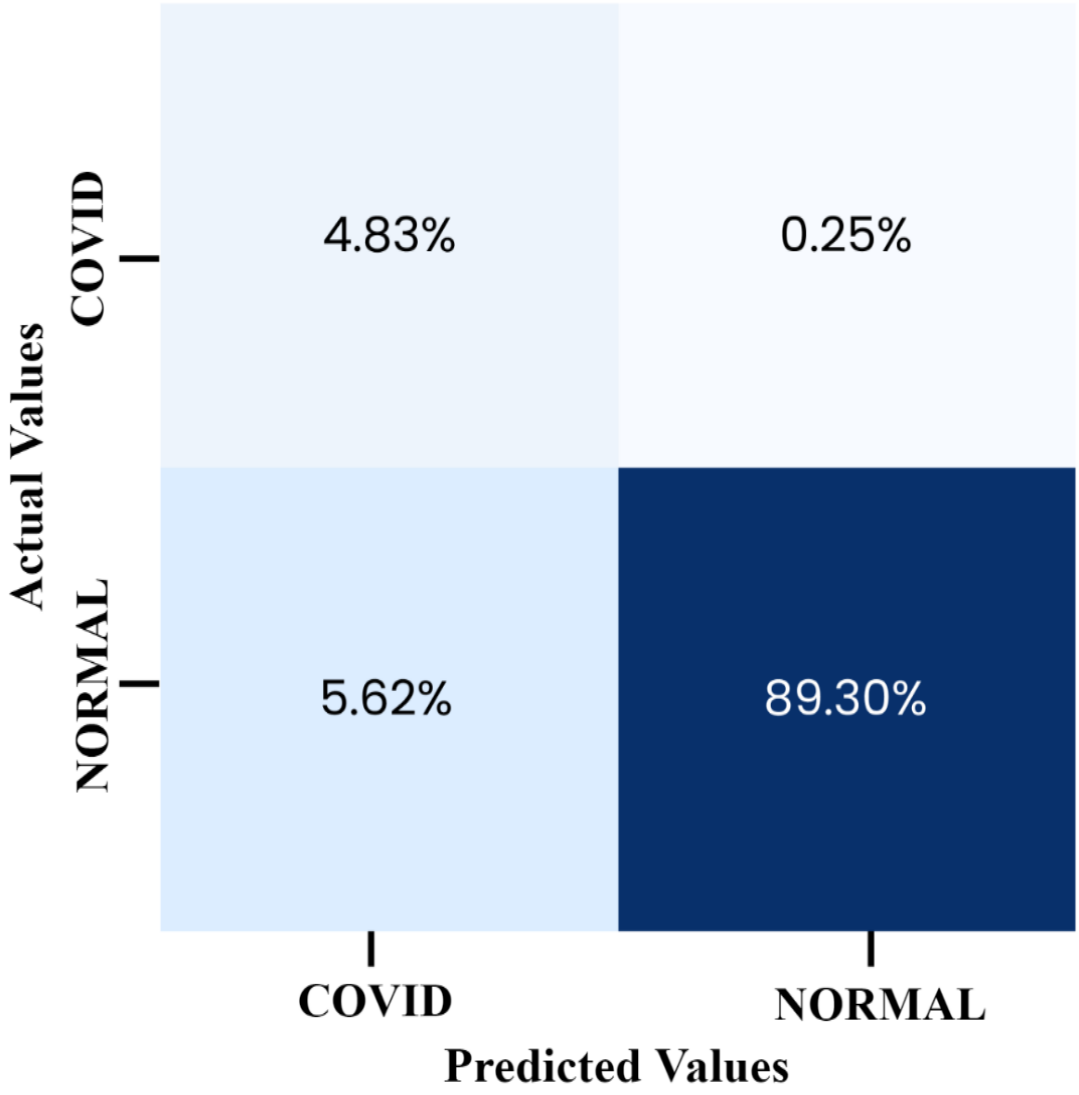

Figure 16: Confusion Matrix showing EffecientNetB0 test evaluation

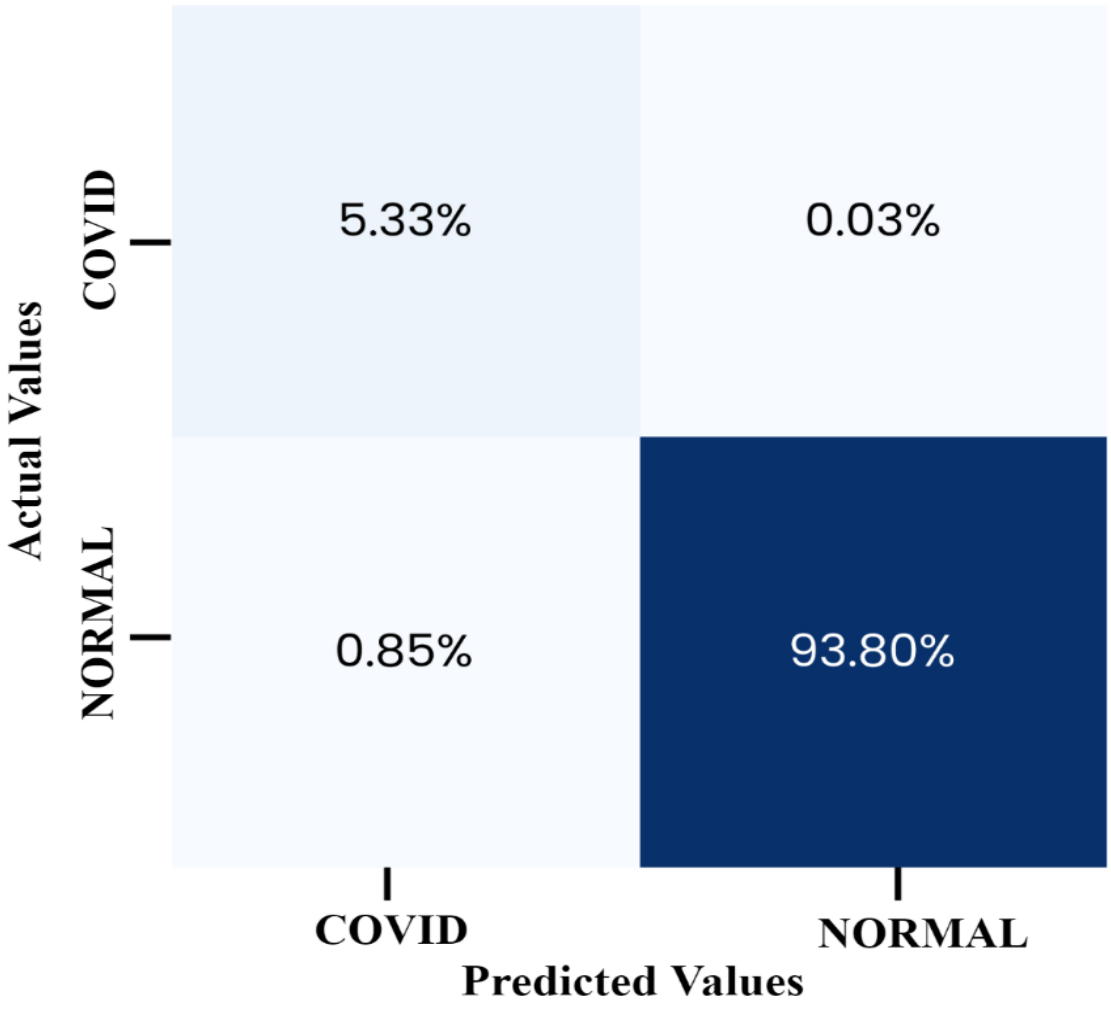

Figure 17: Confusion Matrix showing MobileNetV2 test evaluation

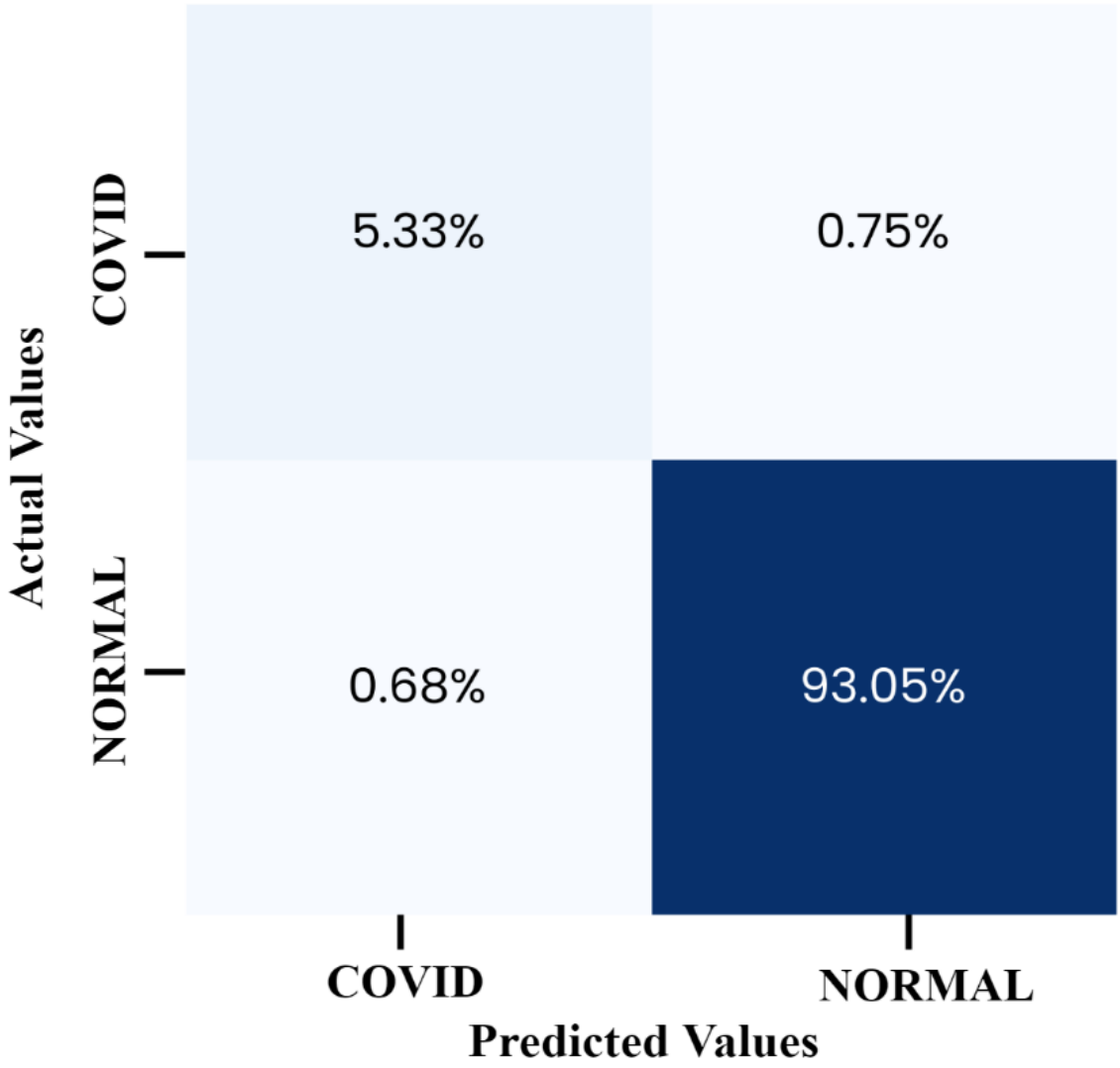

Figure 18: Confusion Matrix showing Xception Net test evaluation

4.2 Identification of Patient Condition

The proposed model for automated detection of coronavirus cases from HRCT images using five different algorithms that takes multiple images as input, processing only those CT images with visible lungs. A deep neural network saves selected images and classifies them as normal or Covid-19 infected. After the selection of threshold, subject's condition can be easily indicated.

Threshold value depends upon model's precision, CT scan images below the threshold are normal, and more than a threshold are taken to be affected by covid-19. A threshold can be set to zero if the trained model is highly accurate. The accuracy of proposed model set the threshold as zero. After image selection if the model detects even only one image as infected, it indicates that the subject is Covid positive. Speed of this fully automated system is represented in Table 7 in terms of training time vis inference time.

Table 7: Training and Inference time of all five models

Model	**Training Time/Epoch** (ms)	**Inference Time/image (ms)**
ResNet50V2	2.9	58
Inception V3	4.2	74
Efficient Net B0	2.4	50
Xception	2.5	55
MobileNetV2	3.4	60

4.3 Feature Visualization

CT scan images were classified into normal and infected by using the Grad-CAM algorithm. The model performance was investigated by high lighting infectious areas, while normal images were identified by the network as non-infected and confirming them as non-covid. In Figure 18 the difference between normal and covid images can be seen easily.

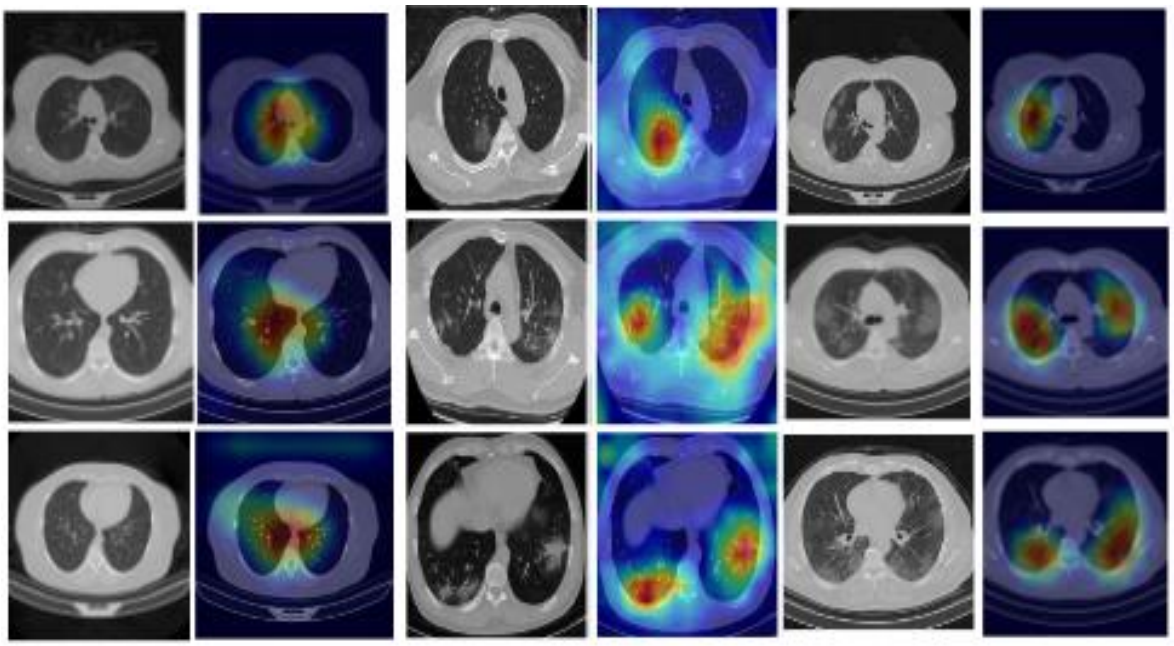

Figure 19: Grad-CAM visualization centrally marked left 2-colums showing 3 normal images while middle 2-columns showing 3 unilateral and right 2-columns showing bilateral infectious area

CHAPTER 5

DISCUSSION

DISCUSSION

Covid-19 image classification used a transfer learning approach, in which five different pre-trained CNN networks, ResNet50V2, Inception V3, Efficient Net B0, Xception, and Mobile NetV2 were used. The proposed model uses 4000 test images with an overall accuracy of 99.9% on ResNet50V2, which is then followed by MobileNetV2, Xception Net, InceptionNetV3, and EfficientNetB0 as 99.1%, 98.5%, 98.4%, and 94.1%, respectively. The achieved accuracy on this open-source data set was 98.49% in a previous study using ResNet50V2 in addition to feature pyramid network on more than 7996 test images, to classify corona infected and normal CT-scan images (Rahimzadeh et al., 2021).

Ahsan, et al., modified MobileNetV2 that upholds best performance with an accuracy of more than 95% on Covid-19 CT images (Ahsan et al., 2021). Advanced inception-based CNN models, classifies CT-scan images using machine learning techniques and demonstrated an accuracy of about 99% (Yamin et al., 2021). Three models out of five achieve higher accuracy than previous results using the same dataset for training and validation. MobileNetV2 gives the highest covid-19 sensitivity values 99.5%, while ResNet50V2 achieves 99.9% for covid-19 specificity and 99% covid-19 precision values. The overall accuracy of all five models is shown in Table 8 and further details can be obtained from Appendix A.

Table 8: Training and Validation Accuracy of five models

Models	Accuracy (%)
ResNet50V2	99.9
InceptionV3	98.4
Efficient Net B0	94.1
Xception	98.5
MobileNetV2	99.1

ResNet50V2 false detections are very low as compared to others. The model used in this study, ResNet50V2 performs patient identification more precisely even when there is a very low Covid threshold. This confirms that model used in this research was able to learn covid infection better than model used in previously studies. The specificity of proposed

technique suggested that it can also be applied to other medical image classification tasks. This network achieves more accurate results with faster execution time and lesser memory requirements. However, parameter tuning was required incorporating hyperparameter searching techniques. To avoid overfitting, substantial training instances were given to the network. Training data, exclusively learn essential features and is applicable when suitable data is available on various 2-D types of pathological classes.

Grad-CAM algorithm was implemented to process binary classification for visualizing sensitive extracted features. In Figure 6, it can be easily observed that non infected normal images have been marked in the center whereas Covid-19 infected cases have been heat-mapped in the infected areas. Hence, the proposed model not only validates classification of infected and/or normal cases but also suggests the extent of infection by highlighting affected areas. If both lobes of the lungs are infected, both sides of lungs are highlighted thus significantly defining the spread of disease.

Moreover, as it can be seen in Table 3, processing speed of proposed model is adequately high. ResNet50V2 being most time cost effective exhibiting 2.5 ms training per epoch and inference time of 58 ms and MobileNetV2 being highest in terms of processing time, consuming 3.4 ms for training per epoch and 66 ms as inference time. In some cases, the Covid-19 precision is not high as its accuracy, e.g precision value of EffecientNetB0 and InceptionV3 is 46.1% and 79%, respectively for the covid-class whereas their accuracy is 94.1% and 98.4%, respectively. Details of precision values can be found in Appendix A. The probable cause of this void can be unbalanced distribution of test data set.

Certain limitations still exist in this work as the proposed classification model is not evaluated on some other validation sets. Further research is needed to evaluate proposed model by using other medical image classification tasks independent of this data set. This research does not make any prior assumptions about image classification. Test data set need to be equally divided for better precision values. Furthermore, by extending hyper parameter tuning and further training epochs, it would be possible to improve the model's generalization ability. This will lead to address challenges in computer-aided diagnosis (CAD) system implementation. In the future, proposed architecture can be modified into a 3-Dimensional CNN model to evaluate its performance in other medical imaging tasks.

Further research to develop CAD models of proposed networks is required to achieve greater optimization.

CHAPTER 6

CONCLUSION

CONCLUSION

A CNN-based architecture to classify normal and Covid-19 infected images by using the HRCT dataset is proposed. Five different pre-trained models were used to evaluate best optimized performance. Accuracy of three out of these five models was improved. ResNet50V2 with an accuracy of 99.9% proved to be the best option for detection of Covid-19 infections. The accuracy of other two models MobileNetV2 and XceptionNet was achieved to be 99.1% and 98.5% respectively that is also higher than previously reported values using same dataset. Inception achieved 98.4% accuracy that is equal to previously reported results. However, EfficientNetB0 proved to be last choice with an accuracy of 94.1%. Further research to develop CAD models of proposed networks is required to achieve greater optimization. The same models can also be implemented for automatic and accurate detection of other diseases, using images from different diagnostic modalities.

CHAPTER 7

REFERENCES

REFERENCES

Abbas, A., Abdelsamea, M. M., & Gaber, M. M. (2020). DeTrac: Transfer learning of class decomposed medical images in convolutional neural networks. *IEEE Access*, *8*, 74901–74913. https://doi.org/10.1109/access.2020.2989273

Ahsan, M. M., Nazim, R., Siddique, Z., & Huebner, P. (2021). Detection of COVID-19 patients from CT scan and chest X-ray data using modified mobilenetv2 and lime. *Healthcare*, *9*(9), 1099. https://doi.org/10.3390/healthcare9091099

Altman, D. G., & Bland, J. M. (1994). Statistics notes: Diagnostic Tests 2: Predictive values. *BMJ*, *309*(6947), 102–102. https://doi.org/10.1136/bmj.309.6947.102

Anwar, T., & Zakir, S. (2020). Deep learning based diagnosis of COVID-19 using chest CT-scan images. https://doi.org/10.36227/techrxiv.12328061

Arab-Mazar, Z., Sah, R., Rabaan, A. A., Dhama, K., & Rodriguez-Morales, A. J. (2020). Mapping the incidence of the COVID-19 hotspot in Iran – implications for travellers. *Travel Medicine and Infectious Disease*, *34*, 101630. https://doi.org/10.1016/j.tmaid.2020.101630

Arpaci, I., Huang, S., Al-Emran, M., Al-Kabi, M. N., & Peng, M. (2021). Predicting the COVID-19 infection with fourteen clinical features using machine learning classification algorithms. *Multimedia Tools and Applications*, *80*(8), 11943–11957. https://doi.org/10.1007/s11042-020-10340-7

Belouzard, S., Chu, V. C., & Whittaker, G. R. (2009). Activation of the SARS coronavirus spike protein via sequential proteolytic cleavage at two distinct sites. *Proceedings of the National Academy of Sciences*, *106*(14), 5871–5876. https://doi.org/10.1073/pnas.0809524106

Belouzard, S., Millet, J. K., Licitra, B. N., & Whittaker, G. R. (2012). Mechanisms of coronavirus cell entry mediated by the viral Spike protein. *Viruses*, *4*(6), 1011–1033. https://doi.org/10.3390/v4061011

Bosch, B. J., van der Zee, R., de Haan, C. A., & Rottier, P. J. (2003). The coronavirus spike protein is a class I virus fusion protein: Structural and functional characterization of the Fusion Core Complex. *Journal of Virology*, *77*(16), 8801–8811. https://doi.org/10.1128/jvi.77.16.8801-8811.2003

Channappanavar, R., Zhao, J., & Perlman, S. (2014). T cell-mediated immune response to respiratory coronaviruses. *Immunologic Research*, *59*(1-3), 118–128. https://doi.org/10.1007/s12026-014-8534-z

Chaudhary, S., Sadbhawna, S., Jakhetiya, V., Subudhi, B. N., Baid, U., & Guntuku, S. C. (2021). Detecting covid-19 and community acquired pneumonia using chest CT scan images with Deep Learning. *ICASSP 2021 - 2021 IEEE International Conference on Acoustics, Speech and Signal Processing (ICASSP)*. https://doi.org/10.1109/icassp39728.2021.9414007

Chen, Y., Guo, Y., Pan, Y., & Zhao, Z. J. (2020). Structure analysis of the receptor binding of 2019-ncov. *Biochemical and Biophysical Research Communications*, *525*(1), 135–140. https://doi.org/10.1016/j.bbrc.2020.02.071

Chollet, F. (2017). Xception: Deep learning with depthwise separable convolutions. *2017 IEEE Conference on Computer Vision and Pattern Recognition (CVPR)*. https://doi.org/10.1109/cvpr.2017.195

Falzone, L., Gattuso, G., Tsatsakis, A., Spandidos, D., & Libra, M. (2021). Current and innovative methods for the diagnosis of COVID-19 infection (review). *International Journal of Molecular Medicine*, *47*(6). https://doi.org/10.3892/ijmm.2021.4933

Fang, Y., Zhang, H., Xie, J., Lin, M., Ying, L., Pang, P., & Ji, W. (2020). Sensitivity of chest CT for covid-19: Comparison to RT-PCR. *Radiology*, *296*(2). https://doi.org/10.1148/radiol.2020200432

Federico, C., Andrea, C., Davide, F., Chiara, D. R., Daniele, C., Eleonora, S., Alessandra, C., Elena, D. V., Giuseppe, B., Massimo, L., & Anna, C. (2020). Development, evaluation, and validation of machine learning models for COVID-19 detection based on routine blood tests. https://doi.org/10.1101/2020.10.02.20205070

Girshick, R., Donahue, J., Darrell, T., & Malik, J. (2016). Region-based convolutional networks for accurate object detection and segmentation. *IEEE Transactions on Pattern Analysis and Machine Intelligence*, *38*(1), 142–158. https://doi.org/10.1109/tpami.2015.2437384

Guan, W.-jie, Ni, Z.-yi, Hu, Y., Liang, W.-hua, Ou, C.-quan, He, J.-xing, Liu, L., Shan, H., Lei, C.-liang, Hui, D. S. C., Du, B., Li, L.-juan, Zeng, G., Yuen, K.-Y., Chen, R.-chong, Tang, C.-li, Wang, T., Chen, P.-yan, Xiang, J., … Zhong, N.-shan. (2020). Clinical

characteristics of Coronavirus Disease 2019 in China. New England Journal of Medicine, 382(18), 1708–1720. https://doi.org/10.1056/nejmoa2002032

Han, J., Brown, C., Chauhan, J., Grammenos, A., Hasthanasombat, A., Spathis, D., Xia, T., Cicuta, P., & Mascolo, C. (2021). Exploring automatic covid-19 diagnosis via voice and symptoms from crowdsourced data. *ICASSP 2021 - 2021 IEEE International Conference on Acoustics, Speech and Signal Processing (ICASSP)*. https://doi.org/10.1109/icassp39728.2021.9414576

He, K., Zhang, X., Ren, S., & Sun, J. (2016). Deep residual learning for image recognition. *2016 IEEE Conference on Computer Vision and Pattern Recognition (CVPR)*. https://doi.org/10.1109/cvpr.2016.90

Huang, C., Wang, Y., Li, X., Ren, L., Zhao, J., Hu, Y., Zhang, L., Fan, G., Xu, J., Gu, X., Cheng, Z., Yu, T., Xia, J., Wei, Y., Wu, W., Xie, X., Yin, W., Li, H., Liu, M., … Cao, B. (2020). Clinical features of patients infected with 2019 novel coronavirus in Wuhan, China. *The Lancet*, *395*(10223), 497–506. https://doi.org/10.1016/s0140-6736(20)30183-5

Howard, A. G., Zhu, M., Chen, B., Kalenichenko, D., Wang, W., Weyand, T., ... & Adam, H. (2017). Mobilenets. *Efficient convolutional neural networks for mobile vision applications*. https://doi.org/10.48550/arXiv.1704.04861

Jin Huang, & Ling, C. X. (2005). Using AUC and accuracy in evaluating learning algorithms. *IEEE Transactions on Knowledge and Data Engineering*, *17*(3), 299–310. https://doi.org/10.1109/tkde.2005.50

Kondu, K., Prerana, A., & Sailaja, K. N. (2022). A deep convolution neural network for detection covid-19 and pneumonia based on the xception and RESNET50V2 algorithm. *International Journal for Research in Applied Science and Engineering Technology*, *10*(6), 1875–1879. https://doi.org/10.22214/ijraset.2022.44147

Krizhevsky, A., Sutskever, I., & Hinton, G. E. (2017). ImageNet classification with deep convolutional Neural Networks. *Communications of the ACM*, *60*(6), 84–90. https://doi.org/10.1145/3065386

Ksiazek, T. G., Erdman, D., Goldsmith, C. S., Zaki, S. R., Peret, T., Emery, S., Tong, S., Urbani, C., Comer, J. A., Lim, W., Rollin, P. E., Dowell, S. F., Ling, A.-E., Humphrey, C. D., Shieh, W.-J., Guarner, J., Paddock, C. D., Rota, P., Fields, B., … Anderson, L.

J. (2003). A novel coronavirus associated with severe acute respiratory syndrome. *New England Journal of Medicine*, *348*(20), 1953–1966. https://doi.org/10.1056/nejmoa030781

Kurihara, K. (2022). Special feature: Statistics for covid-19 pandemic data. *Japanese Journal of Statistics and Data Science*, *5*(1), 275–277. https://doi.org/10.1007/s42081-022-00166-y

Letko, M., Marzi, A., & Munster, V. (2020). Functional assessment of cell entry and receptor usage for SARS-COV-2 and other lineage B betacoronaviruses. *Nature Microbiology*, *5*(4), 562–569. https://doi.org/10.1038/s41564-020-0688-y

Li, B., Li, X., Wang, Y., Han, Y., Wang, Y., Wang, C., Zhang, G., Jin, J., Jia, H., Fan, F., Ma, W., Liu, H., & Zhou, Y. (2020). Diagnostic value and key features of computed tomography in coronavirus disease 2019. *Emerging Microbes & Infections*, *9*(1), 787–793. https://doi.org/10.1080/22221751.2020.1750307

Li, Q., Guan, X., Wu, P., Wang, X., Zhou, L., Tong, Y., Ren, R., Leung, K. S. M., Lau, E. H. Y., Wong, J. Y., Xing, X., Xiang, N., Wu, Y., Li, C., Chen, Q., Li, D., Liu, T., Zhao, J., Liu, M., … Feng, Z. (2020). Early Transmission Dynamics in Wuhan, China, of novel coronavirus–infected pneumonia. *New England Journal of Medicine*, *382*(13), 1199–1207. https://doi.org/10.1056/nejmoa2001316

Li, W., Moore, M. J., Vasilieva, N., Sui, J., Wong, S. K., Berne, M. A., Somasundaran, M., Sullivan, J. L., Luzuriaga, K., Greenough, T. C., Choe, H., & Farzan, M. (2003). Angiotensin-converting enzyme 2 is a functional receptor for the SARS coronavirus. *Nature*, *426*(6965), 450–454. https://doi.org/10.1038/nature02145

Loey, M., Manogaran, G., & Khalifa, N. E. (2020). A deep transfer learning model with classical data augmentation and CGAN to detect COVID-19 from chest CT radiography digital images. *Neural Computing and Applications*. https://doi.org/10.1007/s00521-020-05437-x

Magadum, A., & Kishore, R. (2020). Cardiovascular manifestations of covid-19 infection. Cells, 9(11), 2508. https://doi.org/10.3390/cells9112508

Mahase, E. (2020). Coronavirus: Covid-19 has killed more people than SARS and MERS combined, despite lower case fatality rate. *BMJ*, m641. https://doi.org/10.1136/bmj.m641

Maiese, A., Manetti, A. C., La Russa, R., Di Paolo, M., Turillazzi, E., Frati, P., & Fineschi, V. (2020). Autopsy findings in COVID-19-related deaths: A literature review. Forensic Science, Medicine and Pathology, 17(2), 279–296. https://doi.org/10.1007/s12024-020-00310-8

Martinez-Velazquez, R., Tobón V., D. P., Sanchez, A., El Saddik, A., & Petriu, E. (2021). A machine learning approach as an aid for early COVID-19 detection. *Sensors*, *21*(12), 4202. https://doi.org/10.3390/s21124202

Millet, J. K., & Whittaker, G. R. (2014). Host cell entry of Middle East respiratory syndrome coronavirus after two-step, furin-mediated activation of the spike protein. *Proceedings of the National Academy of Sciences*, *111*(42), 15214–15219. https://doi.org/10.1073/pnas.1407087111

Nishiura, H., Jung, S.-mok, Linton, N. M., Kinoshita, R., Yang, Y., Hayashi, K., Kobayashi, T., Yuan, B., & Akhmetzhanov, A. R. (2020). The extent of transmission of novel coronavirus in Wuhan, China, 2020. *Journal of Clinical Medicine*, *9*(2), 330. https://doi.org/10.3390/jcm9020330

Omori, R., Matsuyama, R., & Nakata, Y. (2020). The age distribution of mortality from novel coronavirus disease (covid-19) suggests no large difference of susceptibility by age. Scientific Reports, 10(1). https://doi.org/10.1038/s41598-020-73777-8

Ou, X., Liu, Y., Lei, X., Li, P., Mi, D., Ren, L., Guo, L., Guo, R., Chen, T., Hu, J., Xiang, Z., Mu, Z., Chen, X., Chen, J., Hu, K., Jin, Q., Wang, J., & Qian, Z. (2020). Characterization of spike glycoprotein of SARS-COV-2 on virus entry and its immune cross-reactivity with SARS-COV. *Nature Communications*, *11*(1). https://doi.org/10.1038/s41467-020-15562-9

Pan, Y., Long, L., Zhang, D., Yuan, T., Cui, S., Yang, P., Wang, Q., & Ren, S. (2020). Potential false-negative nucleic acid testing results for severe acute respiratory syndrome coronavirus 2 from thermal inactivation of samples with low viral loads. *Clinical Chemistry*, *66*(6), 794–801. https://doi.org/10.1093/clinchem/hvaa091

Parikh, R., Mathai, A., Parikh, S., Chandra Sekhar, G., & Thomas, R. (2008). Understanding and using sensitivity, specificity and predictive values. *Indian Journal of Ophthalmology*, *56*(1), 45. https://doi.org/10.4103/0301-4738.37595

Rahimzadeh, M., & Attar, A. (2020). A modified deep convolutional neural network for detecting COVID-19 and pneumonia from chest X-ray images based on the concatenation of xception and resnet50v2. *Informatics in Medicine Unlocked*, *19*, 100360. https://doi.org/10.1016/j.imu.2020.100360

Rahimzadeh, M., Attar, A., & Sakhaei, S. M. (2021). A fully automated deep learning-based network for detecting COVID-19 from a new and large lung CT scan dataset. *Biomedical Signal Processing and Control*, *68*, 102588. https://doi.org/10.1016/j.bspc.2021.102588

Rabi, F. A., Al Zoubi, M. S., Kasasbeh, G. A., Salameh, D. M., & Al-Nasser, A. D. (2020). SARS-COV-2 and coronavirus disease 2019: What we know so far. *Pathogens*, *9*(3), 231. https://doi.org/10.3390/pathogens9030231

Ruan, Q., Yang, K., Wang, W., Jiang, L., & Song, J. (2020). Clinical predictors of mortality due to COVID-19 based on an analysis of data of 150 patients from Wuhan, China. *Intensive Care Medicine*, *46*(5), 846–848. https://doi.org/10.1007/s00134-020-05991-x

Saville, J.W. *et al.* (2022) "Three-dimensional visualization of viral structure, entry, and replication underlying the spread of SARS-COV-2," *Chemical Reviews*, 122(17), pp. 14066–14084. Available at: https://doi.org/10.1021/acs.chemrev.1c01062

Scott, M. (1999). Bias, accuracy, and precision. *Radiocarbon*, *41*(2), 221–222. https://doi.org/10.1017/s0033822200019561

Shah, J. V., Shah, C., Shah, S., Gandhi, N., Dikshit, N. A., Patel, P., Parghi, D., & Pankhania, M. (2021). HRCT chest in COVID-19 patients: An initial experience from a private imaging center in Western India. *Indian Journal of Radiology and Imaging*, *31*(S 01). https://doi.org/10.4103/ijri.ijri_405_20

Shah, S. A., Gajbhiye, M. I., Saibannawar, A. S., Kulkarni, M. S., Misal, U. D., & Gajbhiye, D. I. (2021). Retrospective analysis of chest HRCT findings in coronavirus disease pandemic (covid-19)- an early experience. *Indian Journal of Radiology and Imaging*, *31*(S 01). https://doi.org/10.4103/ijri.ijri_483_20

Shamila Ebenezer, A., Deepa Kanmani, S., Sivakumar, M., & Jeba Priya, S. (2022). Effect of image transformation on EFFICIENTNET model for COVID-19 CT Image

Classification. *Materials Today: Proceedings*, *51*, 2512–2519. https://doi.org/10.1016/j.matpr.2021.12.121

Shamsi, A., Asgharnezhad, H., Jokandan, S. S., Khosravi, A., Kebria, P. M., Nahavandi, D., Nahavandi, S., & Srinivasan, D. (2021). An uncertainty-aware transfer learning-based framework for covid-19 diagnosis. *IEEE Transactions on Neural Networks and Learning Systems*, *32*(4), 1408–1417. https://doi.org/10.1109/tnnls.2021.3054306

Shin, H.-C., Roth, H. R., Gao, M., Lu, L., Xu, Z., Nogues, I., Yao, J., Mollura, D., & Summers, R. M. (2016). Deep convolutional neural networks for computer-aided detection: CNN Architectures, dataset characteristics and transfer learning. *IEEE Transactions on Medical Imaging*, *35*(5), 1285–1298. https://doi.org/10.1109/tmi.2016.2528162

Shu, Z., Zhou, Y., Chang, K., Liu, J., Min, X., Zhang, Q., Sun, J., Xiong, Y., Zou, Q., Zheng, Q., Ji, J., Poon, J., Liu, B., Zhou, X., & Li, X. (2020). Clinical features and the traditional Chinese medicine therapeutic characteristics of 293 COVID-19 inpatient cases. *Frontiers of Medicine*, *14*(6), 760–775. https://doi.org/10.1007/s11684-020-0803-8

Sohrabi, C., Alsafi, Z., O'Neill, N., Khan, M., Kerwan, A., Al-Jabir, A., Iosifidis, C., & Agha, R. (2020). World Health Organization declares global emergency: A review of the 2019 novel coronavirus (COVID-19). *International Journal of Surgery*, *76*, 71–76. https://doi.org/10.1016/j.ijsu.2020.02.034

Soni, M., Gomathi, S., Kumar, P., Churi, P. P., Mohammed, M. A., & Salman, A. O. (2022). Hybridizing convolutional neural network for classification of Lung Diseases. *International Journal of Swarm Intelligence Research*, *13*(2), 1–15. https://doi.org/10.4018/ijsir.287544

Szegedy, C., Vanhoucke, V., Ioffe, S., Shlens, J., & Wojna, Z. (2016). Rethinking the inception architecture for computer vision. *2016 IEEE Conference on Computer Vision and Pattern Recognition (CVPR)*. https://doi.org/10.1109/cvpr.2016.308

Rawat, W., & Wang, Z. (2017). Deep convolutional neural networks for Image Classification: A Comprehensive Review. *Neural Computation*, *29*(9), 2352–2449. https://doi.org/10.1162/neco_a_00990

Tan, M. and Le, Q. (2019). Efficientnet: Rethinking model scaling for convolutional neural networks. *International conference on machine learning*, 6105-6114. Available from https://proceedings.mlr.press/v97/tan19a.html.

Tian, H., Liu, Y., Li, Y., Wu, C.-H., Chen, B., Kraemer, M. U., Li, B., Cai, J., Xu, B., Yang, Q., Wang, B., Yang, P., Cui, Y., Song, Y., Zheng, P., Wang, Q., Bjornstad, O. N., Yang, R., Grenfell, B. T., … Dye, C. (2020). An investigation of transmission control measures during the first 50 days of the covid-19 epidemic in China. *Science*, *368*(6491), 638–642. https://doi.org/10.1126/science.abb6105

Walls, A. C., Park, Y.-J., Tortorici, M. A., Wall, A., McGuire, A. T., & Veesler, D. (2020). Structure, function, and antigenicity of the SARS-COV-2 spike glycoprotein. *Cell*, *181*(2). https://doi.org/10.1016/j.cell.2020.02.058

Who coronavirus disease (covid-19) dashboard. (2020). *Bangladesh Physiotherapy Journal*, *10*(1). https://doi.org/10.46945/bpj.10.1.03.01

Wong, H. Y., Lam, H. Y., Fong, A. H.-T., Leung, S. T., Chin, T. W.-Y., Lo, C. S., Lui, M. M.-S., Lee, J. C., Chiu, K. W.-H., Chung, T. W.-H., Lee, E. Y., Wan, E. Y., Hung, I. F., Lam, T. P., Kuo, M. D., & Ng, M.-Y. (2020). Frequency and distribution of chest radiographic findings in patients positive for covid-19. *Radiology*, *296*(2). https://doi.org/10.1148/radiol.2020201160

Wu, C., Chen, X., Cai, Y., Xia, J., Zhou, X., Xu, S., Huang, H., Zhang, L., Zhou, X., Du, C., Zhang, Y., Song, J., Wang, S., Chao, Y., Yang, Z., Xu, J., Zhou, X., Chen, D., Xiong, W., … Song, Y. (2020). Risk factors associated with acute respiratory distress syndrome and death in patients with coronavirus disease 2019 pneumonia in Wuhan, China. *JAMA Internal Medicine*, *180*(7), 934. https://doi.org/10.1001/jamainternmed.2020.0994

Wu, Z., & McGoogan, J. M. (2020). Characteristics of and important lessons from the coronavirus disease 2019 (covid-19) outbreak in China. *JAMA*, *323*(13), 1239. https://doi.org/10.1001/jama.2020.2648

Xue, S., & Abhayaratne, C. (2021). Covid-19 diagnostic using 3D deep transfer learning for classification of volumetric computerised tomography chest scans. *ICASSP 2021 - 2021 IEEE International Conference on Acoustics, Speech and Signal Processing (ICASSP)*. https://doi.org/10.1109/icassp39728.2021.9414947

Yamin, M., Ahmed Abi Sen, A., Mahmoud AlKubaisy, Z., & Almarzouki, R. (2021). A novel technique for early detection of covid-19. *Computers, Materials & Continua*, *68*(2), 2283–2298. https://doi.org/10.32604/cmc.2021.017433

Zhang, J., Litvinova, M., Wang, W., Wang, Y., Deng, X., Chen, X., Li, M., Zheng, W., Yi, L., Chen, X., Wu, Q., Liang, Y., Wang, X., Yang, J., Sun, K., Longini, I. M., Halloran, M. E., Wu, P., Cowling, B. J., … Yu, H. (2020). Evolving epidemiology and transmission dynamics of Coronavirus Disease 2019 outside Hubei Province, China: A descriptive and modelling study. *The Lancet Infectious Diseases*, *20*(7), 793–802. https://doi.org/10.1016/s1473-3099(20)30230-9

Zu, Z. Y., Jiang, M. D., Xu, P. P., Chen, W., Ni, Q. Q., Lu, G. M., & Zhang, L. J. (2020). Coronavirus disease 2019 (COVID-19): A perspective from China. *Radiology*, *296*(2). https://doi.org/10.1148/radiol.2020200490

APPENDIX A

Test Evaluation with overall accuracy, sensitivity, specificity, and precision values

Models	tp	fp	ctp	cfn	cfp	ntp	nfn	nfp	Overall accuracy %	Covid accuracy %	Normal accuracy %	Covid sensitivity %	Normal sensitivity %	Covid specificity %	Normal specificity %	Covid precision %	Normal precision %
ResNet50V2	3996	4	217	2	2	3779	2	2	99.9	99.9	99.9	99.0	99.9	99.9	99.0	99.0	99.9
Inception V3	3939	61	207	6	55	3732	55	6	98.4	98.4	98.4	97.1	98.5	98.5	97.1	79.0	99.8
Efficient Net B0	3765	235	193	10	225	3572	225	10	94.1	94.1	94.1	95.0	94.0	94.0	95.0	46.1	99.7
Xception Net	3943	57	221	30	27	3722	27	30	98.5	98.5	98.5	88.0	99.2	99.2	88.0	89.1	99.2
Mobile Net V2	3965	35	213	1	34	3752	34	1	99.1	99.1	99.1	99.5	99.1	99.1	99.5	86.2	99.9